A Review of Lithium-ion Battery Electrode Drying: Mechanisms and Metrology

Ye Shui Zhang[*,1,2,3], *Nicola E. Courtier*[2,4], *Zhenyu Zhang*[1,2], *Kailong Liu*[2,5], *Josh J. Bailey*[1,2,6], *Adam M. Boyce*[1,2], *Giles Richardson*[2,4], *Paul R. Shearing*[1,2], *Emma Kendrick*[*2,7], *Dan J.L. Brett*[*1,2]

[1.] Electrochemical Innovation Lab, Department of Chemical Engineering, University College London, London, WC1E 7JE, UK

[2.] The Faraday Institution, Quad One, Harwell Science and Innovation Campus, Didcot, OX11 0RA, UK

[3.] School of Engineering, University of Aberdeen, Aberdeen, AB24 3UE, UK

[4.] Mathematical Sciences, University of Southampton, Southampton, SO17 1BJ, UK

[5.] WMG, University of Warwick, Coventry, CV4 7AL, UK

[6.] School of Chemistry and Chemical Engineering, Queen's University Belfast, Belfast, BT7 1NN, UK

[7.] School of Metallurgy and Materials, University of Birmingham, Birmingham, B15 2TT, UK

([*]Correspondence: d.brett@ucl.ac.uk; e.kendrick@bham.ac.uk; yeshui.zhang@ucl.ac.uk)

Keywords: LIBs, electrode drying process, *In-situ*, metrology, drying mechanism

Abstract

Lithium-ion battery manufacturing chain is extremely complex with many controlable parameters especially for the drying process. These processes affect the porous structure and properties of these electrode films, and influence the final cell performance properties. However, there is limited available drying information and the dynamics are poorly understood due to the limitation of the existing metrology. There is an emerging need to develop new
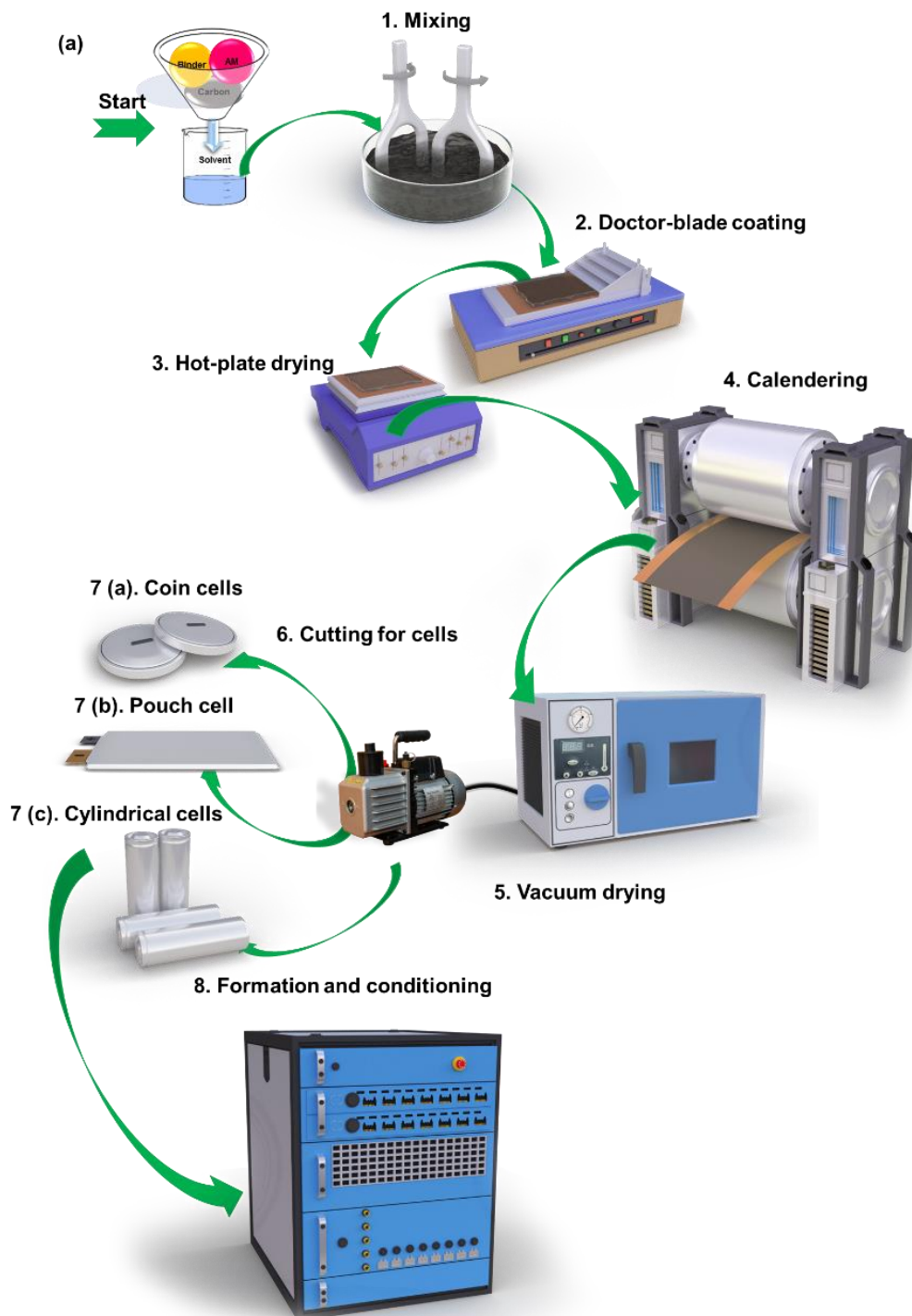
methodologies to understand the drying dynamics to achive improved quality control of the electrode coatings. A comprehensive summary of the parameters and variables relevant to the wet electrode film drying process is presented, and its consequences/effects on the finished electrode/final cell properties mapped. The development of the drying mechanism is critically discussed according to existing modelling studies. Then, the existing and potential metrology techniques, either *in-situ* or *ex-situ* in the drying process are reviewed. It is the intension to develop new perspectives on the application of advanced techniques to enable a more predictive approach to identify optimum lithium-ion battery manufacturing conditions, with a focus upon the critical drying process.

1   Introduction

Lithium-ion batteries (LIBs) are ubiquitous within portable applications such as mobile phones and laptops, and increasingly used in e-mobility due to their relatively high energy and power density. This has led to an exponential increase in batteries being manufactured with a current market size of $34.2 billion (USD) which is expected to grow at a compound annual growth rate of 13.0% from 2020 to 2027.[1] The manufacturing of these batteries has largely been performed in the same way since their initial commercialisation by Sony in the 1990s.[2]

In general, the electrode manufacturing process consists of mixing, coating, drying, calendering, post-drying, and cell assembly steps, as shown in **Figure 1**. The common composites for typical LIB electrodes consist of active materials (AM) with particle sizes of ~10-20 μm, conductive additives with particle sizes of ~100 nm, and binder (polymeric or water-soluble).[3] The active components of the negative and positive electrodes (graphite, and $LiCoO_2$ for the original LIBs, respectively) are mixed separately into a slurry containing a conductive additive, such as carbon black (CB) and a polymeric binder, (polyvinylidene fluoride, PVDF) in a solvent such as N-methyl-2-pyrrolidone (NMP). The carbon binder domain (CBD) promotes mechanical

integrity and electron transport, whereas the pores left by evaporated solvent are filled with electrolyte, promoting lithium-ion transportation, both being directly linked to the performance of the battery through mass transport limitations.[4] The slurry is then tape-cast onto a current collector (CC) (Cu for the negative electrode, and Al for the positive electrode), the resulting coating is then dried to produce a cohesive film which adheres to the CC. The dried electrode is then calendered to reduce the electrode thickness, increasing 3D connectivity, electronic conductivity and maximising the volumetric energy density.[3]
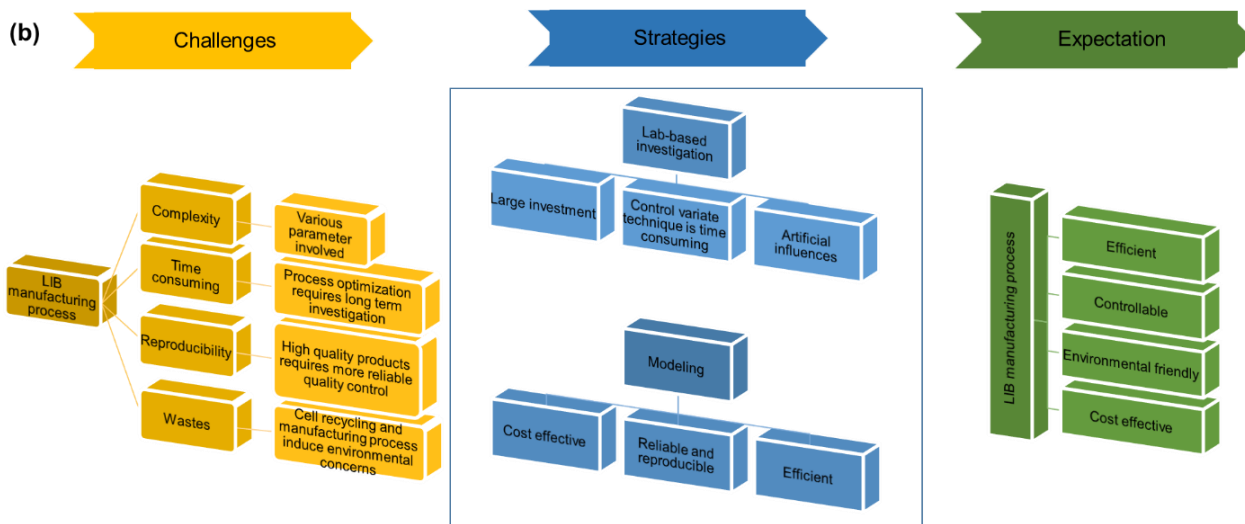
(a)

Start

1. Mixing

Binder

AM

Carbon

Solvent

2. Doctor-blade coating

3. Hot-plate drying

4. Calendering

7 (a). Coin cells

6. Cutting for cells

7 (b). Pouch cell

7 (c). Cylindrical cells

5. Vacuum drying

8. Formation and conditioning

Figure 1 (a) Electrode and battery manufacturing process; (b) the challenges of LIB manufacturing process and the strategies to achieve desirable products.

To achieve consistency within cell electrodes, a homogeneous, defect-free coating is required, with target weights realised throughout the layer. This enables homogeneous current densities and lithium transport between the anode and cathode, improving performance and reducing the propensity for failure. Porosity is required such that ionic diffusion of lithium-ions in the electrolyte occurs, along with electronic conductivity between the active components through the conductive additive, to ensure that electrons can move from the redox-active sites in the active components to the CCs as the battery charges and discharges. The microstructure is important in optimising the electronic and ionic conductivity through the correct electrode architectures. The distribution of the microporous phase, formed by the CB and binder, which partially fills the pores between the electrode particles (AM), improves the mechanical stability of the electrode and improves the electrical contact to the CCs.[4] The microstructure is controlled through the mixing, coating and, most importantly, the drying and subsequent calendering processes.

Although the wet processing of electrodes has developed into a mature technique in the electrode manufacturing industry,[5] there remain unresolved issues with the process, especially coating inconsistency and microstructure defects occurring in the drying process (DP).[6] The

5

DP is affected by the previous slurry mixing step and also correlated to the subsequent calendering process. Researchers assert that the properties of the electrode layer, such as its microstructure and morphology, are strongly dependent on the manufacturing process, especially upon the drying protocol.[6b, 7] Hawley and Li[6b] have reviewed the current state of electrode manufacturing for LIBs and critically discussed the key slurry properties that can be adjusted to optimize wet slurry fabrication. The authors noted that the electrochemical performance of the electrode is not solely affected by slurry rheology, but that the drying parameters also play an important role in determining the electrochemical properties of the finished electrode. The optimal coating rate is sensitive to the specific drying mechanisms. Solvent elimination plays a key role in next-generation smart electrode manufacturing.[6b] To better control the properties of the electrode, it is imperative to improve understanding of the drying dynamic,[8] and thus provide the means for manufacturing tailored electrode architectures that can unlock the further potential of LIBs.[6b]

At the same time, the cost of drying is also an important factor that must be taken into account to optimize electrode manufacturing.[3] Wood *et al.*[9] calculated the possible cost reduction in LIB manufacture based on electrode processing cost, energy consumption, electrode thickness and energy consumption for electrolyte wetting and solid electrolyte interphase (SEI) layer formation. The energy consumption during electrode processing is determined by the solvent type, dispersion of the solid loading, drying temperature, air flow rate and drying time. The authors discuss doubling the thickness of the electrode to reduce the cost of CCs and separators.[9] However, they note that this would also lead to an increase in energy consumption in the DP. It has been reported that around 29% of total energy consumption for manufacturing LIBs comes from the stringent requirements on the facilities needed for the electrode slurry mixing and coating processes.[10] Another 47% of the total process energy derives from the electrode DP, in terms of NMP evaporation and recovery.[11] As noted in,[12] improving the

electrode manufacturing process to reduce both cost and energy consumption is a significant challenge.

Various aspects of the electrode manufacturing process have been the subject of recent studies; these include works on the effects of mixing sequences on the electrode components,[13] mixing tools,[13a, 14] coating,[15] drying,[7a, 7b, 8, 16] calendering[17] and post-drying.[18] To effectively control electrode manufacturing will require a series of advanced analytical techniques which could be compatible with *in-situ* and/or *ex-situ* characterizations,[5d, 17k, 19] particularly in the DP. The influence of drying parameters/variables on the properties of the finished electrode is extremely complex.

In this review, the DP is reviewed and the specific stages and mechanisms of this process discussed, with a critical discussion about the drying mechanism and models, which have been used to understand drying dynamics. The effect of different parameters and variables upon the architecture and resultant physical and electrochemical properties of the electrodes are reviewed and the possible defects and how these can be characterized are considered. Finally, the metrology currently utilised to measure the influence of the drying parameters/variables on the electrode is discussed as well as future improvements and opportunities to apply advanced metrology for the analysis, control and modelling of film drying.

2   Drying mechanism

A typical phase change process during electrode drying is summarized in Figure 2. The slurry phase becomes a semi-slurry as the solvent evaporates followed by further removal of solvent to form a condensed layer of coating, and finally resulting in a compacted solid film coating. The process and mechanisms can be explained through multiple stages which relate to the morphological and physical changes in the coating shown in Figure 2; (a) aggregation, (b) film consolidation, (c) film shrinkage and (d) pore emtyping, segragation and bonding. These stages are controled through the solvent extraction mechanisms and processes as shown in Figure 3. The different processes and mechanisms are critically discussed, and potential models are compared in later section.
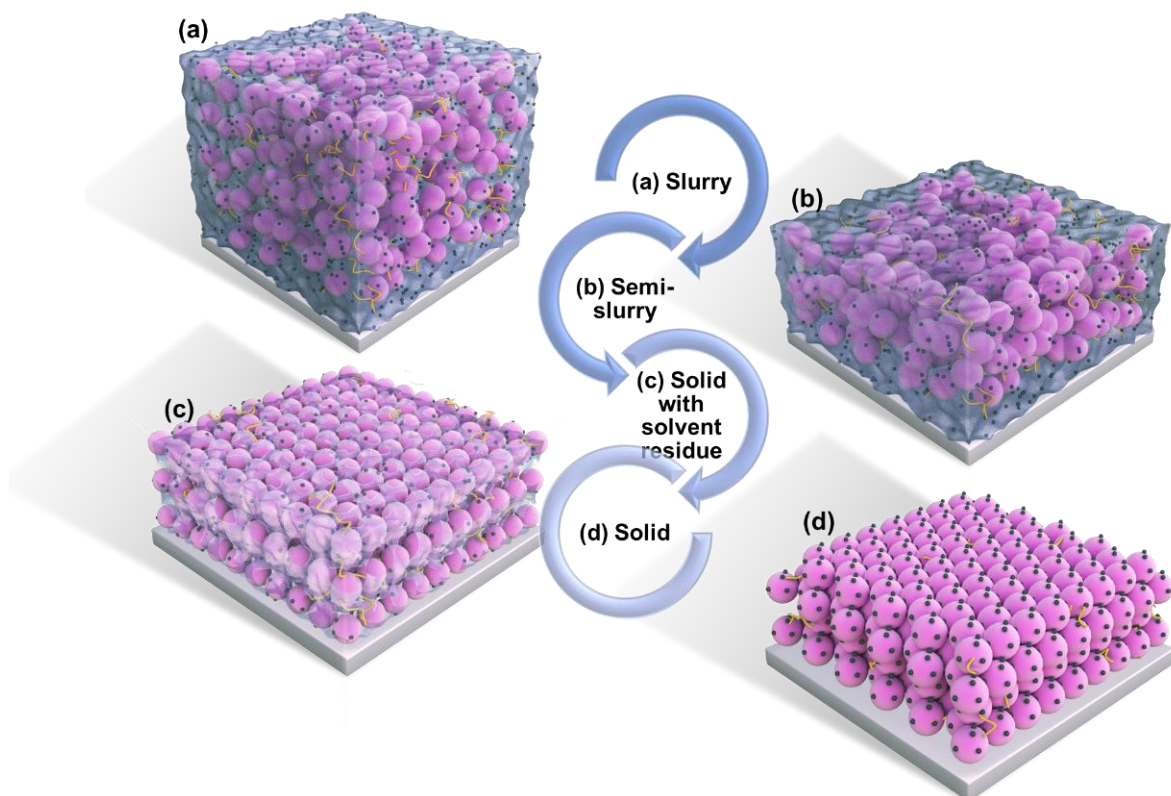
Figure 2 Typical electrode drying process from slurry phase (a) to form a semi-slurry (b), following with the further removal of solvent (c) and end up with a compacted solid film of coating (d) (yellow lines indicate the binder, pink particles indicate active material particles, black dots indicate the conductive carbon and light blue colour indicates the solvent).

2.1 Aggregation

Aggregation is where the particles, solvent and binder coalesce to form the semi-solid coating. The rheological properties of the initial inks are extremely important here, as once the shear from the coating deposition is removed, the inks must form a stable network structure with no flow this coat weight then remains homogeneous with no defects for the subsequent DP. Liu and Mukherjee[20] developed a morphology-detailed mesoscale model to understand the influence of variables, such as active particle morphology and size, volume fraction, solvent evaporation and interactions between the composites. The initial aggregation or film structure model was extrapolated to give further insight into the drying mechanism. The authors proposed both spontaneous aggregation and evaporation-induced aggregation regimes. In this model spontaneous aggregation could be improved with low evaporation rates, which increases the interfacial area compared to evaporation-induced aggregation. This regime could be a potential strategy to optimize the DP in terms of high-quality microstructure.

2.2 Film consolidation

In the second stage of the DP, a semi-slurry is formed, at this point the film consolidates and a surface layer forms on the top of the coating. A top-down film consolidation mechanism was summarized by Jaiser *et al.*.[8] The consolidation layer of the electrode is rapidly formed on the surface of the electrode, even at low density of slurry, with no sedimentation. The consolidation layer grows as the solvent evaporates and the consolidation layer area expands until it approaches the substrate. As the solvent evaporates, binder migration can occur with the solvent, once the shrinkage of the film stops the migration will also stop. Sedimentation does not occur significantly in the battery electrode slurry because of its high viscosity. However, increased temperatures reduce the viscosity of the electrode slurry, which can instigate a low level of sedimentation.[21]

2.3 Film shrinkage/pore emptying

In the third stage of the DP, the binder has a low level of solvent remaining in it, and the final shrinkage of the coating occurs and the final stage of pore emptying. Jaiser *et al.*[16e] hypothesised that during the film shrinkage regime, the solid constituents in the wet film will contact each other to finally form a connected solid layer during shrinkage. The porous structure will form as the backbone of the dry film. The liquid menisci are pinned and play an important role in microstructure evolution since the capillary forces work at the three-phase boundary. Film shrinkage will compete with pore disappearance and the gas-liquid interface regresses from the pore until drying is complete. During the film shrinkage and solvent evaporation stages of drying, the functional additives are mobile and frequently distribute throughout the film.[16e]

2.4 Segregation and bonding

In the final stages of the DP the polymer forms a strong adhesive bond to the substrate, and the final solvent is removed, such that a cohesive strength also forms between all of the particles in the final solid electrode film. Potential segregation of the film can occur and the driving force for this increases with temperature and mass flow rate of the solvent evaporation.[21] Consequently, reduced drying time also leads to a reduced time-to-fixation/time-for-segregation. It has been reported[16a, 22] that the higher degree of polymer entangling would benefit the adhesion strength, and that entanglement may increase with decreasing drying time. The time-to-fixation is also related to the targeted loading, such that the higher the targeted loading the thicker the wet film and more solvent used. Therefore, the time-to-fixation will increase with the increment of the absolute amount of solvent. The term "bonding" is used to describe the process that affects the strength of adhesion of the coating to the substrate, which includes the wetting of the substrate and thermal activation. The increased temperature leads to increased wetting since the surface tension is reduced, based on the Eötvös rules.[21] Thermal

activation here describes the increased diffusion velocity and overcoming of activation energy along with the increased temperature. These two effects boost the interactions between the binder and substrate.

2.5   Solvent evaporation

Solvent evaporation controls the different stages of the DP and hence the morphology of the film. During the electrode DP is generally classified into two phases according to solvent concentration, drying rate and moisture content.[16a, 16i, 23] The first phase is a surface phenomenon as the solid particles are suspended in a pool of the solvent where the evaporation rate has the dominant contribution to the drying rate and is constant until a porous structure is formed. The second phase of drying is much longer than the first phase and more complex.[16i, 23a] Susarla *et al.*[16i] used a continuum-level mathematical model to describe the physical phenomenon of the cathode DP to study solvent removal during the second phase. The mathematical model also took into account mass and heat transfer due to the phase change of the solvent. The finding reveals that most of the solvent (~90 %) removal occurs in the first phase and this process is finished in less than the half of the total drying period. Malcolm *et al.*[23a] describe the two phases of drying subject to the thickness of the electrode coating. The first phase was described as a linear process with a constant evaporation rate to form a compact skeleton of the AM, such that the electrode dimensions at this stage have no significant difference to the final dimensions. The rest of the solvent occurs during the second phase of drying and the re-distribution of conductive additive and binder occur at this stage.

2.6   Comprehensive drying mechanism

Often the drying mechanisms uses the same principals to describe the complete process rather than breaking it down into different mechanisms. In this respect, Westphal *et al.*[21] summarized the DP, including the first drying stages of film consolidation, and the 2nd drying stage of pore

emptying. The further solvent evaporation drives the re-distribution of active and inactive materials and forms a porous network of the coating. The following stage is the segregation that occurs by retreating of the liquid-gas interface in the network. The narrow pores of the AM backbone and the retreating liquid-gas interface may potentially impede the segregation. The last stage is the inactive materials segregate towards the surface of the coating, leading to a depletion of inactive material at the interface between the coating and substrate.[8, 21] Font *et al.*[24] suggest a similar drying mechanism where the DP initiates with film shrinkage during which the solvent evaporates from the surface of the coating, causing shrinkage until the particles of the AM contact each other and stop the coating thickness from further reductions. The second stage is the pore emptying in which the residual solvent in the pores between AM particles evaporates. Jaiser *et al.*[16e] developed a more detailed model to describe the drying mechanism of the electrode based on previous work.[7a],[25] As previous, the first stage of solvent evaporation, driven by capillary forces, leads to film shrinkage and consolidation. Once a solid film is formed from the solid interconnected particles, film shrinkage terminates. Further evaporation of the solvent causes the liquid phase to recede into the porous electrode structure, with subsequent pore emptying. All proposed drying descriptions suggest that the movements of the components in the solvent evaporation stage play a more important role in the formation of the electrode microstructure compared to the pore-emptying stage.[16c, 16f]
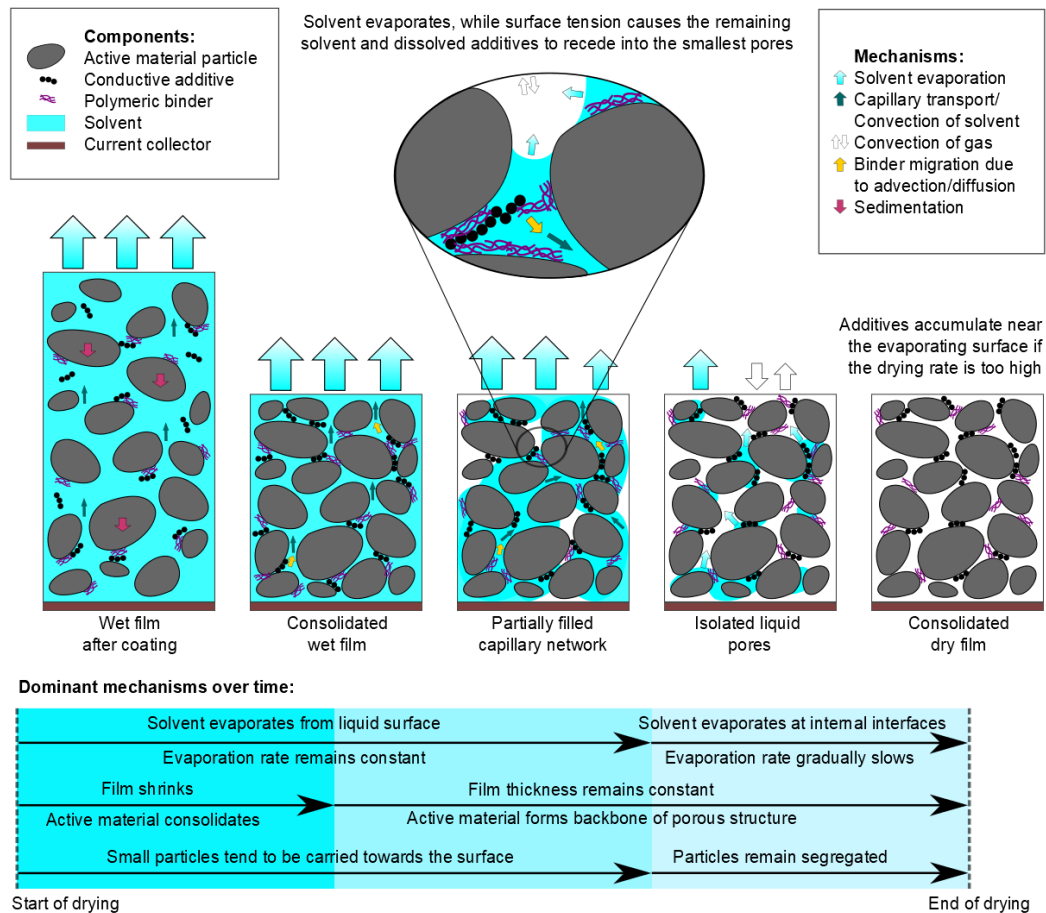
Figure 3 A summary of latest three-stage of drying mechanism which is reproduced from.[26] 2020, Wiley.

3   Parameters and variables that affect battery performance

There are several parameters and factors that affect the quality of the electrode that impact upon the final battery performance; for example, the drying rate, binder types, temperature, drying procedures and formulation. The effects of these factors are discussed in this section.

3.1   Drying Methodologies

As discussed previously, the drying and method of drying the inks and pastes is paramount for establishing the microstructure of the electrodes, cohesion of the film and adhesion to the CC.[3, 19b] Prior to deposition the components of the electrode slurry also require to be well dispersed, and the active components stabilised within a binder and conductive additive matrix, which

13

translates into the electrode upon drying.[3] The most common electrode drying method at the industrial scale is to dry the electrode slurry by large belt dryers with infrared radiators or hot air fans which are installed in the coater and where possible upstream of the dry-room. This is to avoid the remoistening of the cell components post-drying.[5d] For lab-based electrode slurry drying, the conventional air-drying method is to cast the slurry on the CC and dry in an ambient environment or similar mild temperatures. Alternative, high throughput drying methods could revolutionise the LIB electrode manufacturing process. There is significant scope to improve the process, and some examples of alternative methods are suggested form the electro-catalyst as well as the battery industry. Inert gas flow (for air sensitive materials) are for new battery materials such as the high nickel NMC, or the sulfide solid state electrolyte are air sensitive. The materials react with the atmosphere, wither the water or the carbon-dioxide to form residuals on the surface and to degrade the materials. Therefore, modifying the deposition and DP to remove these contaminants may be required. The inert gas may quicken the DP as the heavier gas displaces the solvent during drying.[27],[28] Rotational drying can also speed up the manufacturing, but is limited to electrodes of a particular size and shape, and as such is not currently possible with reel to reel coatings. A well-dispersed is loaded onto the electrode substrate on the inverted rotator, then rotated at speed until the film is completely dry.[27] Spray drying method can achieve high-speed that has been widely applied in many industries as a coating method, such as catalysts, drug carriers, sensors, electronic materials and battery electrodes.[29] Example where this has been used are in silicone-based anodes,[29a] $LiMn_2O_4$ cathode[29b] and Cu_6Sn_5/C composite powders.[29c] The residual water in the electrode can cause unwanted side reactions that influence cell performance. So, the second DP is essential for controlling the water level of the manufactured electrode to less than 100 ppm. The cost of drying is significantly affected by the entire electrode manufacturing process which could be

reduced by attaching additional heating systems, such as infrared, microwave, dielectric heating and laser drying.[3, 30]

3.2 Drying rate

Solvent evaporation in the industrial electrode DP involves a huge expenditure of energy that is a decisive cost factor for manufacturing battery electrodes.[9, 16e, 31] The drying rate is determined by the drying temperature and the air flow rate/velocity.[7a],[16i] Typical drying rates in industrial coating processes are in the range of 25 - 50 m min^{-1}. A fast drying time of 1 to 2 minutes may be required in some particular cases. It should be noted that the capital cost for industrial electrode coating is inversely proportional to the drying rate.[16e] The optimized drying rate during the electrode manufacturing process will promote the balanced binder distribution of electrode film. However, the higher drying rate will result in an uneven distribution of soluble and dispersed binder throughout the electrode, potentially accumulating at the surface.[8, 16a-c] This binder migration can also lead to electrode delamination,[7a, 7b, 16c, 16g] due to the reduction in adhesion strength at the CC-electrode interface. In electrode suspensions with low solid loadings, the AM particles can move within the solvent for much longer and can collide and form agglomerates due to cohesive interaction. Cohesive interaction resulting from capillary pressure due to the surface tension of liquid menisci between particles can cause the formation of cracks.[32] In the case of suspensions with a very low (10 wt.%) solid content, Scheepers *et al.*[32] found that the drying temperature has no significant effect on crack formation.

High temperatures have been reported to potentially lead to greater binder migration, which can cause electrode delamination and result to a high resistance.[7a, 7b, 16c, 16g] Electrode adhesion is strongly dependent upon the drying temperature and that higher temperatures result in lower adhesion strength between the copper CC and the coating layer, as shown for graphite and

LiFePO$_4$ based electrodes.[7a],[7b],[33] Greater segregation of inactive components are observed, which reduce the adhesion strength, and increase the electrical resistance and elasticity. However, the thickness of the coatings need to be also considered, and in the case for graphite,[13] it was observed that the adhesion strength decreases as the drying temperature increases from 80 to 110 °C with mass loadings up to 8.1 g cm^{-2} and adhesion strength decreases when the mass loading is over 10.5 g cm^{-2}. This could be explained as the shorter time-to-fixation is indicative of faster polymer entanglement and subsequently less time for segregation. Adhesion strength was shown to be independent of mass loading, although increasing the drying temperature from 110 to 130 °C resulted in increasing segregation. This situation is thought to be caused by the reduced time-to-fixation as the temperature increases with relatively low mass loading. The situation for higher mass loading is the opposite.[21]

3.3   Binder types

As mentioned previously, typical electrodes are manufactured by applying a thin coating onto a CC, wherein the coating slurry is a mixture of AM, conductive carbon, binder and solvent. The most widely used organic-based binder is PVDF and NMP.[7b, 8, 13b, 13f, 16a] To effectively restrict the volume change, there is a novel dual crosslinked binder has been synthesized from crosslinking esterification reaction of poly(hydroxyethyl methacrylate) (PHM) and polyacrylic acid (PAA) to fabricate Si anode. As one of the most widely used organic-based binder [34], NMP is a costly solvent in the electrode manufacturing process and it is reprotoxic and treated as a restricted substance in the EU.[35] Aqueous solutions/water-based binder could potentially reduce the cost of electrode manufacturing and energy consumption.[9] Water-based processing has been commercialized for graphite anode manufacturing[12] and researchers have extended the approach to the manufacture of cathodes.[36] The coating manufacturing and capital cost on equipment for both water-based and NMP-based electrode drying has been calculated in $ kWh^{-1}. The findings showed that the total costs for electrode manufacturing contribute to 8-

9 % of the total battery pack cost.[11] The authors estimated that a two-times reduction of capital equipment cost could be expected in drying and solvent recovery steps for using water-based solvent compared with NNP-based solvent.[37] The solvent recovery step requires less capital investment, and it is environmental friendly compared with the polymeric-based solvent recovery.[6b, 11, 38] However, although there are advantages for using water-based solvents during electrode manufacturing, there are also disadvantages/challenges related to process ability and cell performance during aqueous electrode processing. The water-based slurry has excessive particle agglomeration, more hydroxyl groups on the coating surface and high surface tension compared with NMP-based slurry.[11] The agglomerate formation for electrodes prepared by an aqueous process is due to the weak van der Waals attractions, or strong electrostatic interactions caused by surface charges.[13i, 39] The strong hydrogen bonding and electrostatic forces promote agglomeration. Therefore, there is a need to add extra dispersant to supply an electrostatic barrier.[6b] The inferior wetting of aqueous slurry on the CC leads to high surface tension and lower adhesion strength that can potentially reduce the cycle life of the cell.[6b, 40] In addition, the aqueous cathode slurry is basic, which could potentially corrode the aluminium CC, and can promote metal dissolution. Moreover, electrodes made from water-based solvents can lead to more cracking without optimum drying protocols[11, 40b],[41] and it has been reported the challenges induced by aqueous processing are more serious for slurries containing nickel-rich AM.[42] Susarla *et al.*[16i] compared the energy demand for drying water-based solvent coatings and concluded that it is nearly 10 times less than for organic-based solvent coatings. Li and Wang[16a] investigated binder concentration distributions in dried water-based (carboxymethyl cellulose, CMC) and organic-based (PVDF) LiCoO$_2$ electrode sheets and the electrode properties in terms of physical, electrical and electrochemical properties. The experimental results showed the electrode made of organic-based binder had a non-uniform distribution of the electrode components, and to an extent worse than that for the

electrode made of water-based binder. They also predicated the binder distribution in the dried electrode based on theoretical calculations of migration-controlled drying kinetics, indicating that the organic-based binder has higher non-uniform distributed electrode constituents compared with the water-based electrode layer. This resulted in the electrode prepared with organic-based binder having weaker CC adhesion and higher electrical resistance.

Apart from the conventional electrode manufacturing process, a self-healing silicon microparticle anodes for high-energy LIBs has been investigated,[43] which is rely on the ability to repair damage spontaneously that is an important survival feature in nature because it increases the lifetime of most living creatures. The authors highlighted this feature is highly desirable for rechargeable batteries because the lifetime of high-capacity electrodes (e.g. silicon anodes) is shortened by mechanical fractures generated during the cycling process.[43] A novel water-based conductive binder PF-COONa is reported by Liu *et al*.[44] for high-performance silicon anodes in LIBs, which can form strong chemical bond with the Si particles and ensures the electrode mechanical integrity and electronic conductivity.

3.4   Thickness and mass loading

The formulation, mass and mass balance of the electrodes directly relate to battery performance. The gravimetric and volumetric energy density of LIBs can improve through improved manufacturing factors, such as a reduction in the amount of inactive material, reduction of pore volume, thinner separator, less CC and hence thicker electrode layers.[9, 17g, 45] For example with thicker electrode, the ratio of active component to CC is higher, less electrode cutting is required and a lower number of electrodes in the stack which results in lower manufacturing costs [4]. Another method of increasing the energy density is to reduce the inactive components in the electrode formulation (binder and conductive additive) in the electrode. The decrease of the active-to-inactive material ratio will lead to an increase of electrical resistance and an

optimum ratio is required for improved electrode and cell performance.[46] Westphal et al.[21] found the resistance, adhesion strength and elasticity stay constant with an inactive material ratio higher than 12 wt.%. Zheng et al.[46] investigated the cooperation between AM, binder and conductive carbon in a LIB cathode. The authors reported the total inactive material amount and binder-to-conductive additive ratio significantly affects the porosity, conductivity, specific capacity, first Coulombic efficiency, and rate capability of the electrodes. However, Westphal et al.[21] found higher mass loading leads to greater segregation of inactive materials within the electrode and poor adhesion, which can be solved with lower drying temperatures.

3.5   Modelling of drying parameters and variables

As a consequence of the complexity of the DP, involving coupled mechanical and chemical mechanisms, numerous parameters are variables are required to describe the system, as discussed in Sections 3.2-3.5. These parameters/variables play a direct and vital role in affecting the properties of dried intermediate products; which, in turn, further determine the properties of final manufactured batteries.[26] Understanding the individual or combined effects of these parameters/variables on the finished electrodes is of great importance to the optimization and improvement of the dried intermediate product qualities. The main approach to analysing interdependencies among the various drying parameters and variables is still based on trial and error. In light of this, reliable and flexible models to achieve effective analyses of drying parameters/variables and predict dried intermediate product properties are urgently required.

To date, several modelling techniques have been adopted to perform analysis of different drying parameters/variables. To uncover how the DP affects the distributions and interactions of components in the electrode composite, Liu et al.[20] proposed a mesoscale morphology model to analyse the particle morphology properties as well as solvent evaporation dynamics,

while their effects on the constituent phase distribution of LIBs electrode were also explored. The results illustrate that better aggregation with conductive additive particles could be obtained with smaller isometric active particles. Through considering more forces on the mesoscale particles, such as contact friction and solvent-caused damping force, a dynamic particle packing model was proposed to forecast the microstructure of slurries and dried films.[47] As the DP can easily cause spatial in-homogeneities within the electrode component distribution, further leading to the reduced battery performance, Font *et al.*[24] constructed an electrode drying mathematical model to predict and track the binder distribution evolution. Existing modelling techniques for prediction of drying parameters/variables are mainly based on the mechanism models which use the physical or chemical equations to describe the drying dynamics. Few attempts have been made to utilise interpretable machine-learning methodologies to analyse parameters for the electrode DP.

In order to improve the qualities of LIBs with high energy density, a quality planning strategy to identify the interactions between process and product along the whole battery production chain was proposed by Westermeier *et al.*.[48] Several active parameters/variables (temperature, number of heating cycles, etc.) and passive parameters/variables (moisture content, thickness difference, adhesion, etc.) from the DP were identified and analysed based on the failure mode and affect the data analysis solution; then, drying parameters with a significant effect on the cell quality could be chosen for quantifications by experiments or data-driven models. With the rapid development of cloud-computing platforms and artificial intelligence, data-driven solutions are becoming powerful tools to conduct sensitivity analyses of battery production. Several studies have been carried out through designing suitable data-driven models such as neural networks,[49] decision trees[50] and support vector machines[51] to predict and analyse the interdependencies of parameters for battery manufacturing processes, such as mixing and coating. However, to our best knowledge, no attempt has been applied for parameter analysis

of the DP. Note that the DP will also generate numerous parameters and data, so designing the effective data-driven models to analyse the correlations and importance of drying parameters is a recommended research direction.

3.6 Coating defects and influences on the electrode and battery performance

Coating defects are caused by inhomogeneities in the ink, or due to the limitations between the coating and the DPs. Pin holes, cracks, delamination and inhomogeneities can in general be controlled by the speed of the coating and of drying. Figure 4 shows the cause and effect for the different defects.
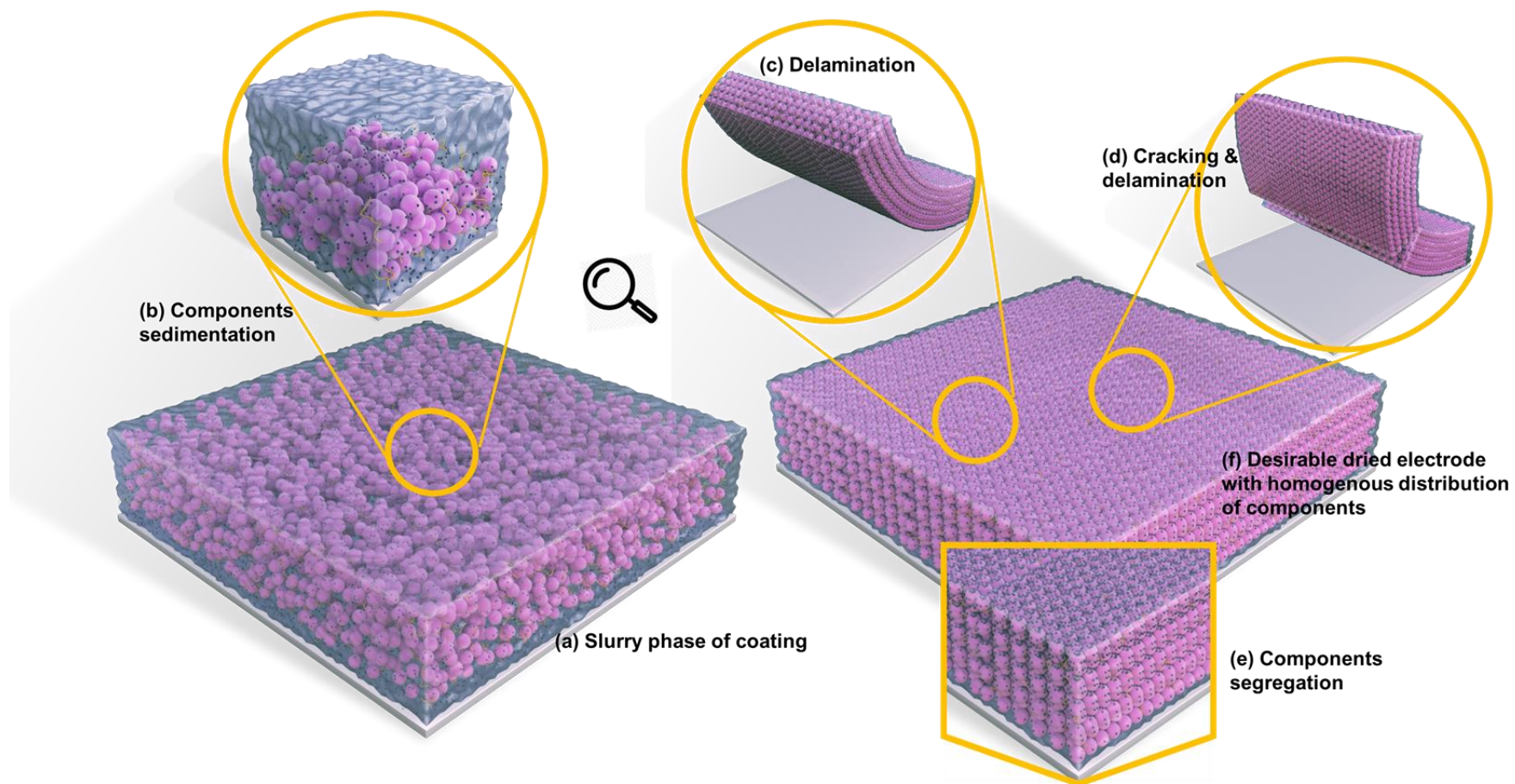
Figure 4 Schematic diagrams of the electrodes with coating defects. (a) Slurry phase of coating; (b) components sedimentation; (c) delamination of coating from current collector; (d) coating cracking and delamination; (e) components segregation; (f) desirable dried electrode coating with homogenous distribution of components.

- **Binder migration and delamination,** can be controled through drying conditions (**Figure 4c**). High temperature leads to binder migration to the surface of the electrode reducing adhesion, and causing inhomogeneous distribution of the binder and delamination of the electrode.[8, 24] The heterogeneous distribution of binder will also affect the electrochemical performance, including the internal resistance and associated rate capability as the binder acts as a barrier for lithium-ion insertion.[6b, 16b, 16c, 16g, 23a, 52]

- **Component segregation, Figure 4(e).** Component segregation of the binder and conductive additive in an electrode leads to binder and CB concentrations that decrease from the top to the bottom of the coating.[21] The segregation increases as the drying temperature and the amount of solvent used increases. CB was shown to be more concentrated at the top surface region of the coating and decreases linearly from top to bottom at a low drying rate.[16h] Component segregation reduces the adhesion strength between the electrode coating and the CC/substrate, as well as inducing a substantial increase in the electrical resistance and elasticity.

- **Film shrinkage and cracking.** Shrinkage of the electrode film is normally caused by solvent evaporation from the porous structure influences the evolution of the microstructure and re-distribution of the components, such as the binder.[16e] Shrinkage leads to drying stress development, consequently causing coating cracking, curling and delamination. Water-based solvents, and thicker electrodes tend to have greater cracking issues, particulalry at faster drying rates.[26] Figure 4(d) is a model of cracking of the electrode coating.

The parameters which influence the properties of the LIB electrodes during the DP and the corresponding consequences is summarised in Figure 5. During the DP, a series of parameters affect electrode properties, including the drying rate, binder types and formulation. The drying rate is controlled by the temperature, pressure, radiation intensity and airflow, depending on the type of drying method. The types of binder directly correlate with the drying time, as the slurry made from water-based binder would take a relatively shorter time to dry out the coating comparing with the slurry made from an organic-based binder. There are different defects generated by different drying conditions, such as binder migration of the electrode coating, delamination of the coating layer from the CC, electrode film shrinkage and the component segregation of the coating. Correspondingly, these defects will affect the microstructure of the formed electrode, adhesion strength between the electrode coating and the CC, cell capacity, resistivity and cycling performance.
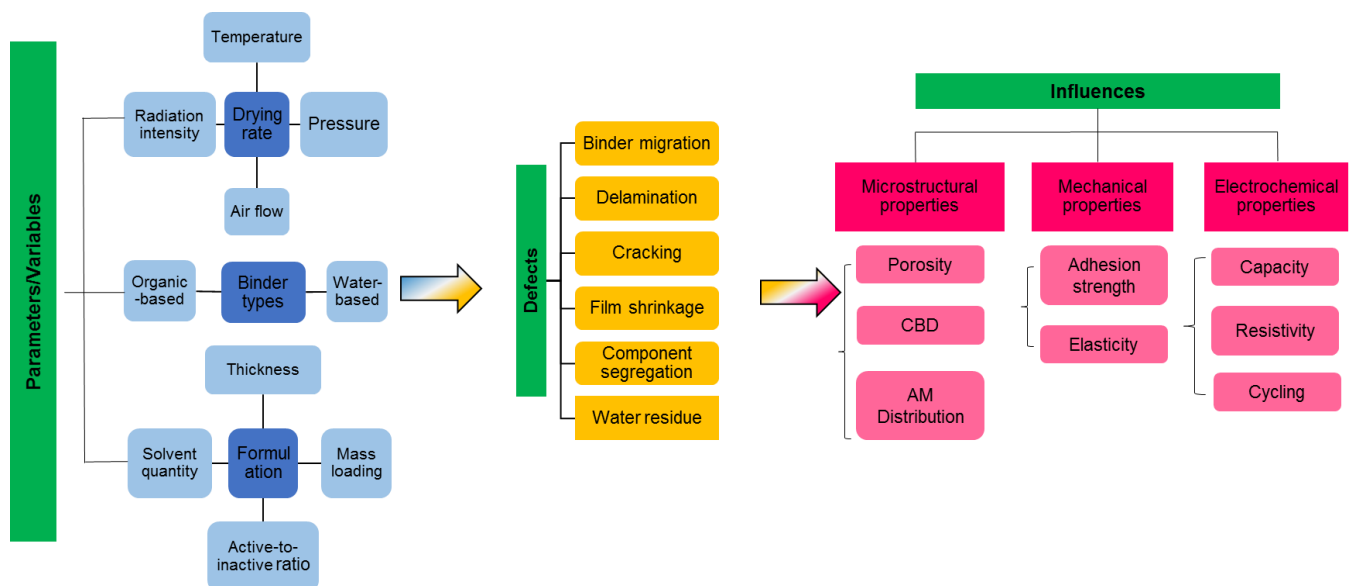

Figure 5 Summary of the parameters/variables which can affect the electrode formation during the DP and corresponding issues and consequences.

The drying mechanisms during the DP are complex and the electrochemical performance of the formed electrodes are dominated by different drying parameters, such as drying rate, binder type and formulation, as shown in Figure 5. To optimize the DP during electrode manufacture,

all of the parameters should be considered.[16d, 16i] In order to control the DP, metrology measurements are needed to understand the effect of the input variables upon the outputs. Section 4 details the metrology tools currently available to study the electrodes in greater detail.

4 Electrode drying metrology

Various types of metrology have been applied in the DP to study the drying mechanism, which are all based on different principles and have different resolutions as shown in Table 1. These are very powerful techniques that have been applied to LIB electrodes DP. Some of them have been introduced in the LIB electrode DP either as *ex-situ* or *in-situ* methods to investigate the electrode microstructure evolution or component distributions.

Although some of the metrology have been briefly reviewed for characterizing the morphology of LIB electrodes after DP *ex-situ*,[53] as shown in Figure 6 (a). There are very limited details about the existing metrology, such as capability of the methods for carrying out *in-situ* investigation, resolutions and targeting applications for investigation LIB electrode DP. As listed in Table 1, we were not only summarizing the existing metrology which have been used in the LIB electrode DP, but also including the emerging metrology that have potential to be introduced in the DP to support the in-depth understanding of drying dynamics.

The reviewed metrology is grouped according to its capability and types as shown in Table 1 and Figure 6 (a). The outlook of each method for investigating the LIB electrode DP is also included in this section, as a guidance for the researchers to find the most relevant and suitable method to assist the research. These include; *In-situ/Operando* characterization methods to characterize LIBs in terms of electrochemical reactions and degradation mechanisms. A variety of spectroscopy and microscopy techniques for elucidation of chemical and physical properties.[54]
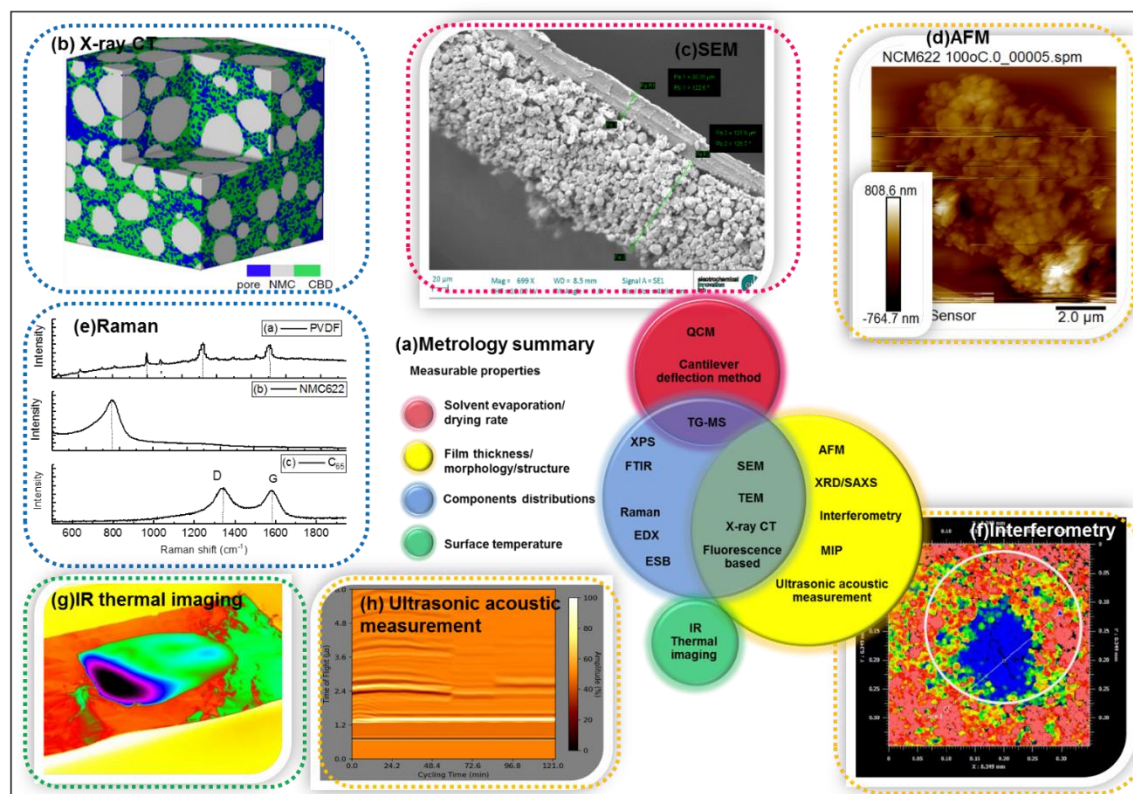
Figure 6 (a) The reviewed metrology grouped by the capability of measuring the different key parameters during the electrode drying process; (b) an example of cathode characterized by X-ray CT and the resolved pores, NMC as active material (AM)) and the carbon binder domain (CBD) which was reproduced from.[55] 2020, Nature; (c) examples of micrograph of LIBs cathode dried at 120 °C scanned by a Zeiss EVO 10 scanning electron microscope; (d) an example of AFM analysis for NMC622 cathode coating dried at 100 °C; (e) Raman spectra for a typical LIB cathode composite material, NMC622, PVDF and C_{65}, recorded between 100 and 3500 cm^{-1} (514 nm) with a laser power of 10 mW; (f) an example of interferometry result for the surface roughness analysis of NMC622 coating which was dried at room temperature; (g) an example of the surface temperature profile of a cathode coating obtained by IR thermal camera; (h) an example of in-line ultrasound acoustic measurement of cathode coating drying at 40 °C.

4.1 Metrology for characterizing LIB electrodes

Most of the metrology measurements current are based upon *ex-situ* measurements.

Atomic force microscopy (AFM) has been widely used as a tool to measure the surface roughness and morphology of coatings (Figure 6) (d). Although highly sensitive, it is not expected that AFM techniques can be integrated into drying metrology measurements due to the high sensitivity of the machine to vibrations. Advanced AFM systems not only probing surface properties such as morphology,[56] but also mechanical (e.g., elastic modulus),[57] electrical (e.g., conductivity, permittivity)[58] and functional properties[59] (e.g., piezoelectric response) *etc.*.[56a]

Cantilever deflection is an *in-situ* method which could offer improved quality control upon coatings and DPs.[60] Here, stress development of the electrode during drying can be measured, using a cantilever, laser, position sensing detector and data recording system.[61] This is significantly larger scale (micro-scale depending on the size of the laser spot) compared to AFM (nano-scale or micro-scale).

Interferometry has the highest sensitivity among several phase-sensitive methods which is a powerful tool for non-destructive three-dimensional observations. It can measure surface roughness, thickness and quantitatively visualize the salt concentration distributions that arise in electrolytes during battery operation.[62] Figure 6 (f) is an example of interferometry result for the surface roughness and defect analysis of cathode coating which was dried at room temperature. As a technique with fast data acquisition ability, interferometer could be further applied as an *in-situ* method to investigate the surface evolution of the LIB electrode during DP.

Infrared (IR) thermal imaging as a temperature mapping method has been used to study operational LIBs.[63] The IR thermal images can be obtained with a non-contact IR thermal

camera to detect the thermal radiation and convert it to electrical signals for processing thermal images or videos.[64] Although the IR thermal imaging results could be affected by the radiation from object, atmosphere and surrounding object,[65] this may be resolved by altering the position of the IR camera by 45°.[66] It has been reported that thermal sensitivities of 0.03-0.09 °C within the temperature range of 0-120 °C could be achieved,[63b, 63d] and the spatial resolutions of 0.1-0.3 mm could be attained.[63f, 67] Figure 6 (g) is an example of the surface temperature profile of a cathode coating obtained by IR thermal camera, which could be used to learn about solvent evaporation and surface temperature variation.

Mercury intrusion porosimetry (MIP) has been used to measure the pore size distribution of the dried anode film. This is a quantitative technique which is capable of analysing a large volume (marco or over) of the LIB electrode to obtain a more representative porous structure in both nano- and micro- scale resolutions.

Light based methods are difficult to use in black slurries, as the light waves are absorbed by the slurry components. But can be used for polymeric coatings. Multi-speckle diffusion wave spectroscopy (MSDWS) is a technique based for light scattering which has been developed to study colloidal material properties during DP by measuring the size, molecular weight and relaxation of the particles.[68][69] Fluorescence-based imaging/microscopy has been used to image the latex particle migration within graphite electrode slurry during the DP,[16b] this demonstrated the vertical particle distribution of the coating through the characterization of the fluorescent light intensity. Jaiser *et al.*[16e] further developed the electrode drying mechanism model of electrode coating by imaging the fluorescent light of the coating at different drying times with a single-lens reflex camera equipped with a macro object lens. This could be further developed to incorporate with more advanced metrology to able acquiring more dynamic information simultaneously.

X-ray diffraction (XRD) is a powerful technique to characterize the crystallinity of materials and it has been widely used to characterize electrode materials.[70-72] Conventional synchrotron or neutron scattering can obtain information for the non-equilibrium phase behaviour of colloids that the synchrotron beams are horizontally emitted from the source [73]. There are limited applications of using conventional synchrotron or neutron scattering in colloidal suspension DP which is intrinsically settled horizontally to the ground due to the gravity, such as spry DP,[74] sessile drops[25] or dip coating.[75] Synchrotron X-ray beams have been used to vertically pass through thin films to probe the structural change of colloidal suspensions, which requires special design of the setup.[76]

Vertical small-angle X-ray scattering (SAXS) has been developed as an *in-situ* tool to investigate drying behaviour of charge-stabilized colloidal silica.[77] It has been reported the solidification of the colloidal particles perform ordering at the beginning stage of the drying, and then followed by an immediate aggregation which was driven by capillary pressure and thermal motion of the particles. The further application of this metrology has been extended to fuel cell electrode related study. Kusano *et al.*[78] used contrast-variation small-angle neutron scattering (CV-SANS) to perform a structural evaluation of a catalyst ink for polymer electrode fuel cell electrodes during the DP. This technique shows the great potential to investigate the structural change of the crystallographic compositions in a nano-scale resolution during LIB electrodes during DP.

Raman spectroscopy has been used to quantitatively analyse the binder distribution in LIB anodes during the freeze-drying process.[16c] The coating was taken out of the drying oven at different drying stages for freeze-drying, and subsequently underwent Raman analysis to quantify the binder concentration through the cross-sections of the coating. Drying at 150 °C resulted in a higher concentration of the binder at the surface of the coating compared with that at room temperature.[16c] Applications of Raman technique have been reviewed in more detail

[79]. The spatial resolution of Raman spectrometers coupled with an optical microscope can approach micro-scale. Figure 6 (e) demonstrates the Raman spectra for a typical LIB cathode composite materials, NMC622, PVDF and C_{65}, which proves the capability to study binder distribution for both LIBs cathode and anode.

Scanning electron microscopy (SEM) with associated add-ons is a powerful technique which has been widely applied to characterize the electrode, especially for the microstructure of the electrode materials and distribution of the elements in the different components, as shown in Figure 6 (c).[16a, 16f, 23a, 27, 70c, 80] Li and Wang[16a] used SEM to characterise the microstructure of graphite electrodes, and map the binder concentration distribution in electrodes formed from different types of binders (water-based and organic-based). Malcolm *et al.*[23a] used SEM with energy-dispersive X-ray spectroscopy (SEM-EDX) to analyse the microstructure of electrodes by scanning their top and the bottom to study the mechanism of the DP due to solvent evaporation. TEM can investigate structural and compositional information with atomic resolution.[81] Kusano *et al.*[78] used TEM micrographs to support their assumption that there is significant structural change of electrodes during the DP, especially cracking.

The energy-selective back (ESB) detector is able to identify the light elements but also the same element with different phases, especially for carbons, such as graphite, diamond and amorphous carbon.[82] The further application of this detector has been investigated by Pfaffmann *et al.*,[16h] they introduced a novel technique to enhance the contrast of fluorine-rich regions by using the ESB detector to easily distinguish the CB in graphite electrodes. The authors then use this technique to investigate the CB distributions in cross-sections of graphite electrodes to find out the influences of the drying temperature on the CB distributions during electrode DP.[52a]

Thermogravimetric analysis (TGA) can be used to quantify the areal distribution of binder residue in the manufactured electrodes made of different binders (organic-based and water-based) through selective analysis of different parts of the electrode.[16a] TGA is the most simplest and easy access technique to study the thermal dynamic change of LIB electrode slurry according to the different thermal stability of the composition.

Quartz crystal microbalance (QCM) is one of the common bulk acoustic wave sensors capable of monitoring mass change with nanogram resolution. The oscillating frequency shift can be converted to mass change on the sensor surface using the Sauerbrey equation.[83] As a sensitive mass sensing metrology, there is potential to apply QCM in the LIB electrode DP to monitor the solvent evaporation in a nano-scale resolution to correlate it with the microstructural evolution or fluid dynamics during DP.

Ultrasound acoustic based technique has been widely applied as a battery diagnostic tool to study the battery during operation. The application of ultrasound acoustic technique provides the potential to further apply in LIB electrode DP for drying dynamic studies, as the most dominant change during DP is physical change such as the solvent evaporation, density and porosity of the electrode coating etc. Figure 6 (h) is an example of *in-situ* ultrasound acoustic measurement of cathode coating drying at 40 °C, which the time-of-flight change corresponds to the physical properties change of the electrode slurry coating. The technique is scalable and simple and has significant potential for future applications as an *in-situ* method for LIB electrode drying dynamic study as recently demonstrated.[84]

X-ray photoelectron spectroscopy (XPS) is a powerful surface chemistry characterisation technique, which can quantify the surface elemental compositions of coatings with a depth of ~5 nm.[52a, 70b] Zang *et al.*[52a] studied the migration of styrene butadiene latex during the drying of coating suspensions using XPS.

X-ray radiography has been used to study the dynamic drying behaviour of electrode slurries consisting of SiO_x, CB and CMC in a water-based binder solution.[85] The authors took a horizontal slice of the radiograph through the base of a volume reconstruction of a dried drop consisting of SiOx and SUPER C_{45} in a solution of CMC and deionized water. A series of X-ray radiographs were taken during the electrode slurry DP for calculating the spatial distribution of AM. Non-uniform distribution of active particles formed very quickly, and heating could boost the uniformity of active particles distribution in the early stage of slurry drying.

Different scales of *X-ray computed tomography (X-ray CT)* have been applied extensively to characterize the microstructure of the electrodes after drying.[45, 86] [87] [88] Mapping the 3D microstructure of electrodes is important for understanding the structural heterogeneity and its corresponding effects on battery performance. X-ray CT has been applied *in-situ* to determine the microstructure evolution during battery degradation.[55, 63e, 89] As the porosity of LIB electrode is normally formed during the drying stage during solvent removal. X-ray CT has great potential to study the porosity evolution during the DP.

High-throughput X-ray CT can indirectly track the lithium diffusion during the degradation process and the neutron CT can directly identify lithium diffusion during electrode wetting by an electrolyte.[90] Lu *et al.*[55] have developed a full microstructure-resolved 3D model based on an X-ray nano CT dual-scan superimposition technique to accurately correlate the microstructure and performance, which can be used to investigate the microstructure evolution, porosity and tortuosity as shown in Figure 6(b), which could also assist electrode manufacturing monitoring and control. Dynamic Lithium distribution upon dendrite growth and shorting revealed by *operando* neutron imaging has been studied,[91] to observe the dynamic distribution of Li flowing from the anode to cathode during charge which is induced by the internal short circuit due to Li dendrite growth.

4.2 Summary of electrode metrology

Various techniques have been used to characterize electrodes and investigate the influence of DP (to LIB electrodes DP or electrochemical power source electrode systems or other similar viscoelastic slurry DP) on their properties. Some of the techniques are *ex-situ* methods, the measurement made after drying, such as AFM, fluorescence-based imaging/microscopy, optical interferometry, SEM, TEM, EDX, XRD and MIP.[6b, 16a, 16e, 16f, 23a, 27, 70c, 78, 80, 92] Some of the techniques have been successfully used as *in-situ* methods to study the evolution of the electrode during DP in terms of binder and particle distributions, microstructure, drying rate and drying stress development.[16a-c, 16h, 60, 78, 85] The techniques used for *ex-situ* analysis of the electrode after drying are typically used to investigate the macrostructure and microstructure of the electrode. Table 1 is a summary of the reviewed metrology which either applied in electrode DP, or emerging and potential metrology that can be applied in the LIB electrode DP. Each of the technique may only be suitable for one electrode or both, depending on the individual equipment running environment and feasibility of the experimental setup.

Possible advanced metrology tools which could be applied to the DP are QCM, IR-imaging, X-ray CT, Raman and ultrasound. QCM could be used to support the investigation of solvent evaporation rate during LIB electrode DP in a nano-resolution. IR thermal imaging allows the investigation of surface temperature changes to help optimise heat pulsing effects and process temperature. MSDWS could be used to monitor particle movement in electrode slurry. X-ray CT is capable for characterizing 3D microstructure evolution. Raman spectroscopy could help to identify binder distribution throughout the electrode coating as an *in-situ* method with further development. Ultrasound acoustic technique may be able to acquire physical dynamics of the electrode for a long period, as the signal responses are very quick.

Table 1 Summary of metrology applied in electrode drying process or emerging and potential metrology that can be applied in the LIB electrode drying process.

Metrology	Type	Scale	Environment	*Ex-situ* applications	*In-situ* applications
AFM	Scanning probe microscopy	nm-µm	Inert/ambient	Surface morphology, roughness;[70c, 92] Morphology,[56a, 56c] mechanical,[57] electrical,[58] functional properties[59]	Morphology[56b] and mechanical property[56d]
Cantilever deflection method	Scanning probe microscopy	µm or over	25 ± 1 °C and 20% of relative humidity	N/A	Drying stress development[60]
EDX	Spectroscopy	%	Vacuum	Element composition and distribution[16f, 23a, 27, 80a]	N/A
Fluorescence-based imaging /microscopy	Microscopy	mm	Ambient	Drying mechanism, liquid distribution[16e]	Microstructure change[16b]
MIP	Quantitative	nano	Vacuum	Pore size distribution[6b]	N/A
Optical interferometric profilometry	Optical metrology	nm-cm	Ambient	Surface morphology and thickness[27]	N/A
Raman spectrometer	Quantitative	µm	Ambient	SEI formation,[93] structural characterization of carbon materials[79a]	Binder distribution;[16c] phase transition and Lithium-ion intercalation into graphite;[94] [95]
SEM/TEM	Electron microscopy	nm-µm	Vacuum	Surface morphology and microstructure;[16a, 16f, 23a, 27, 70c, 80] [12, 96] CB distribution;[16h] particle and surface morphology[78]	Cryo-SEM for microstructure evolution;[16b] structure and morphology[79, 148, 149]
TGA/TG-MS	Thermogravimetry	µg	Ambient/programmed heating	N/A	Drying rate, binder distribution[16a]
X-ray CT/ Radiography	Tomographic	nm-cm	Ambient	N/A	Particle distributions[85]
XRD/SAXS/ CV-SANS/neutron CT	X-ray scattering	nm	Ambient	Microstructure of the particles[70]	Crystallographic evolution;[71] [72] [70a, 97] structural change;[77] structure evaluation,[78] electrolyte[98]
QCM	Mass measuring metrology	ng	Ambient	N/A	BF_4^- intercalation into graphite;[97b] SEI thickness and viscoelastic properties [99]
FTIR	Spectroscopy	%	Ambient	N/A	SEI evolution and oxygen-containing groups evolution[95, 100]
IR Thermal imaging	Thermography	µm	Ambient	N/A	Surface temperature[63e]
MSDWS	Spectroscopy	µm	Ambient	N/A	Particles movement in colloidal slurry/suspension[68a, 68b, 68d, 69]
Ultrasound acoustic technique	Acoustic metrology	ns	Ambient	N/A	Physical dynamics;[101] lithium plating on anode;[102] electrodes lithiation and delithiation[103]
XPS	Spectroscopy	ppm	Vacuum	Chemical composition;[70b, 96-97] binder distribution[52a]	Chemical features (qualitative and quantitative)[56c]

5   Challenges and future perspectives

5.1   Drying mechanism models and insights

In the field of electrode drying, continuum-level mathematical modelling can test hypotheses and identify the key physical mechanisms that influence the DP and the quality of the final electrode. The goal is to establish a model that accurately describes how properties of the slurry and drying conditions control each part of the DP. Once such a model has been established, the ultimate aim is to provide a fast and reliable method to predict the optimal drying conditions for different types of electrode slurry.

From previous work as discussed above in section 2 and Figure 3 it is known that the drying mechanism follow several stages. Each of these stages can be modelled, and measurements based upon the metrology for *in-situ* drying can be used to parameterise these models.

1. As the solvent at the surface evaporates, more solvent is transported upwards toward the surface. The removal of solvent from between the AM particles causes them to consolidate.

2. The final aspects of stage one are when the pore volume begins to empty. This is observed from a change in the film surface. Often the end of stage one is where any film shrinkage stops, however in some cases further consolidation particularly for small particles sizes occurs until the solvent in surface porosity is also removed.

3. After the pore empties, a second constant rate solvent evaporation is observed, with transport towards the surface via capillary action. Large pores therefore empty preferentially to smaller pores.

4. Finally, the remaining solvent evaporates and is transported in the gaseous phase through the electrode microstructure to the surface. This drying phase can be faster and does not results in any particle or binder movement.

Cardinal *et al.*[104] proposed a one-dimensional (1D) model that included Brownian diffusion, sedimentation, and evaporation to study the drying of a model system comprised of monodisperse silica particles in water. Buss *et al.*[80d] proposed a 1D model for the transient concentration profiles of particles and soluble polymer in a drying suspension, that involved sedimentation, evaporation and diffusion. They studied a model system of poly(vinyl alcohol) (PVA), silica particles and water. Routh *et al.*[105] derived a governing equation for the evolution of particle volume fraction. They obtained numerical solutions for various Peclet numbers and an asymptotic solution for large Peclet numbers.

Recently, Susarla *et al.*[16i] proposed a 1D model for solvent removal during the electrode DP has been discussed in section 2. They used an established volume-averaging technique proposed by Whitaker *et al.*[106] to develop a macroscopic model. The porous structure formed from the AM is assumed to be in a continuum and each dependent variable is averaged over a small representative volume. The model variables were temperature, partial pressure of vapour and liquid saturation of the pore network. Convective transport of the liquid solvent, gas-phase solvent and air was modelled *via* Darcy's equation, while diffusion of the gases was modelled according to Fick's Law. The transport equations were coupled to an equation for the conservation of energy. The solvent evaporation rate was expressed as a function of saturation, temperature and porosity. The capillary pressure also depended on temperature *via* the surface tension [16i]. However, notably, this work does not consider the process of binder migration and so conclusions drawn from this model are unable to take into account or explain the influence of binder migration on film properties, such as adhesion.

A summary of the latest three-stage drying mechanism is illustrated in Figure 3. Here, two 1D, continuum-level models of the DP are compared.[24] Each of these models is valid only for part of the DP (either the initial film shrinkage stage or the subsequent pore emptying stage) and

involves a subset of the physical mechanisms that have been shown to play an important role in the dynamics of electrode drying. As a result of these limitations, neither model can wholly explain the experimental evidence for a three-part DP presented in.[16d] The optimal drying strategies proposed by Susarla *et al.*[16i] and Font *et al.*[24] appear not to be consistent as the first suggests increasing, while the second suggests decreasing, the drying rate during a multi-stage DP. However, the conclusions from the work of Susarla *et al.*[16i] are drawn only from a model of the pore emptying stages of drying, while those of Font *et al.*[24] apply only to the initial film shrinkage stage. Therefore, these conclusions are not necessarily contradictory and each may explain part of the proposed three-stage optimal drying protocol.[16d]

However, neither of these existing models[16i, 24] can be relied upon to predict the whole optimal LIB electrode DP. The three-stage procedure determined in the experimental study that manages to reduce the total drying time while maintaining good mechanical properties in the final dry electrode coating (in particular adhesion between the electrode film and CC), thereby increasing the efficiency of the drying step.[16d] There is a need to create a more comprehensive and more reliable model to understand the electrode drying mechanism, therefore to predicate the optimal drying protocol for different compositions and formulations for LIB manufacturing.

In summary, the key mechanisms to consider in models of LIB electrode drying are the consolidation of the active particles, the convection/evaporation of the solvent, the advection and diffusion of inactive material (both the binder and conductive additives), and the development of stress/cracking. In contrast to the drying of other particulate coatings, the process of sedimentation appears to have a negligible effect on electrode drying performed at industrially relevant drying rates. Therefore knowledge of the electrode structure, solid content, pore size (solvent content) can be applied to estimate transport speeds and mechanisms. For example capillary transport can be expressed by Darcy's law (permeability multiplied by the

gradient of capillary pressure).[107] A review of past and remaining challenges in pore network modelling in drying technology is presented by Metzger *et al.*[108] Many other industries also require insight into dehydration of porous materials, and a comprehensive review is available for food is available.[109] This highlights that many of techniques and methods are applicable to electrode manufacturing and there are significant opportunities to translate methodologies from other industrial practices. There are many opportunities for improved control and monitoring of this DP. Models can incorporate measured parameters to provide insight in real time changes in the process. One example to improve the DP would be to control the initial DP through solvent transport in the electrode through lower solvent contents in the slurry and monitoring the process through *in-situ* measurements– optimising the drying temperatures and air flow. Then hasten the process in the final stage with a fast drying method (IR-drying for example) to remove the final solvent in the vapour phase. Often the metrology is not used during the DP due to the difficulties in incorporating these tools into the drying area. Significant opportunities are around the integration of measurement techniques, particularly to measure film thickness, coat weight, and also incorporate optical techniques into the drying area to monitor and control the DP.

5.2   Discussions and perspectives of electrode drying metrology

There are three primary methods that have been used to study the electrode DP.[6b] Electrochemical performance of the electrodes which has the benefit of directly correlating the drying parameters with electrochemical performance of LIBs. However, it is not a way to guide the manufacture to optimise the DP with an understanding of the drying mechanism. Experimental studies using different metrology/characterisation techniques, as discussed in Section 4. or computer simulations, which require preliminary experimental results. Simulations and modelling are a faster way to evaluate the drying scenario and provide insight into the DP.[16i] Parameters such as colloidal stability, heat and mass transfer coefficients can

provide useful data for the early stage of electrode manufacturing.[20, 47] Current *in-situ* characterisation examples include microstructure evolution, drying rate, binder and particles distribution or drying stress development, however the drying dynamic information acquired is very limited due to limitations of the different techniques.[16a-c, 16h, 60, 78, 85] Figure 6 and Figure 7 summarise the techniques that have been used to study electrode DP and the prospective techniques that could be introduced in the DP to study drying dynamics. As summarized in Figure 5, there are various parameters/variables during the DP that can lead to different defects of the final electrodes to subsequently affect the cell performance. Therefore, the early stage characterizations of the electrode post-drying could be indicative of the final cell performance. Figure 6(a) illustrates the reviewed metrology grouped by the capability of measuring the different key parameters (solvent evaporation/drying rate; film thickness/morphology/structure; components distributions/surface temperature) during the electrode DP. The drying dynamics of wet electrode slurry coatings are complex and still poorly understood. *Ex-situ* metrology does not provide real time data, and significant opportunities are available to expand current in-situ monitoring. There is an emerging need to introduce and develop more advanced metrology techniques to study the DP. The in-depth understanding of the effects of drying parameters/variables on electrode formation by directly observing the DP will not only help understand the mechanism of the DP, but also contribute to the next generation of electrode design for LIBs to achieve the electrode quality control in the early stage of LIB manufacturing.

6   Conclusion

In this review, the DP of Li-ion battery electrodes has been considered and the effect of different parameters/variables on the architecture and properties of resultant electrodes were discussed. A critical review of different drying mechanisms and models are included with a view to understanding drying dynamics. However, no single model can be relied upon to predict the whole electrode drying procedure. The three-stage drying regime is aiming to

reduce the total drying time and also maintaining good mechanical properties of dried electrode coating (in particular adhesion between the electrode film and CC), thereby increasing the efficiency of the drying step. The need to create more comprehensive models to study the electrode drying mechanism is identified. Meanwhile, a broad range of metrology also have been reviewed and grouped according to its capabilities, scales and other characteristics of the metrology. This would guide the researchers for employing a broader range of metrology tools to study and monitor the LIB electrode manufacturing process with specific requirement. Therefore, to contribute to the next generation of electrode design for LIBs with a more controllable process.
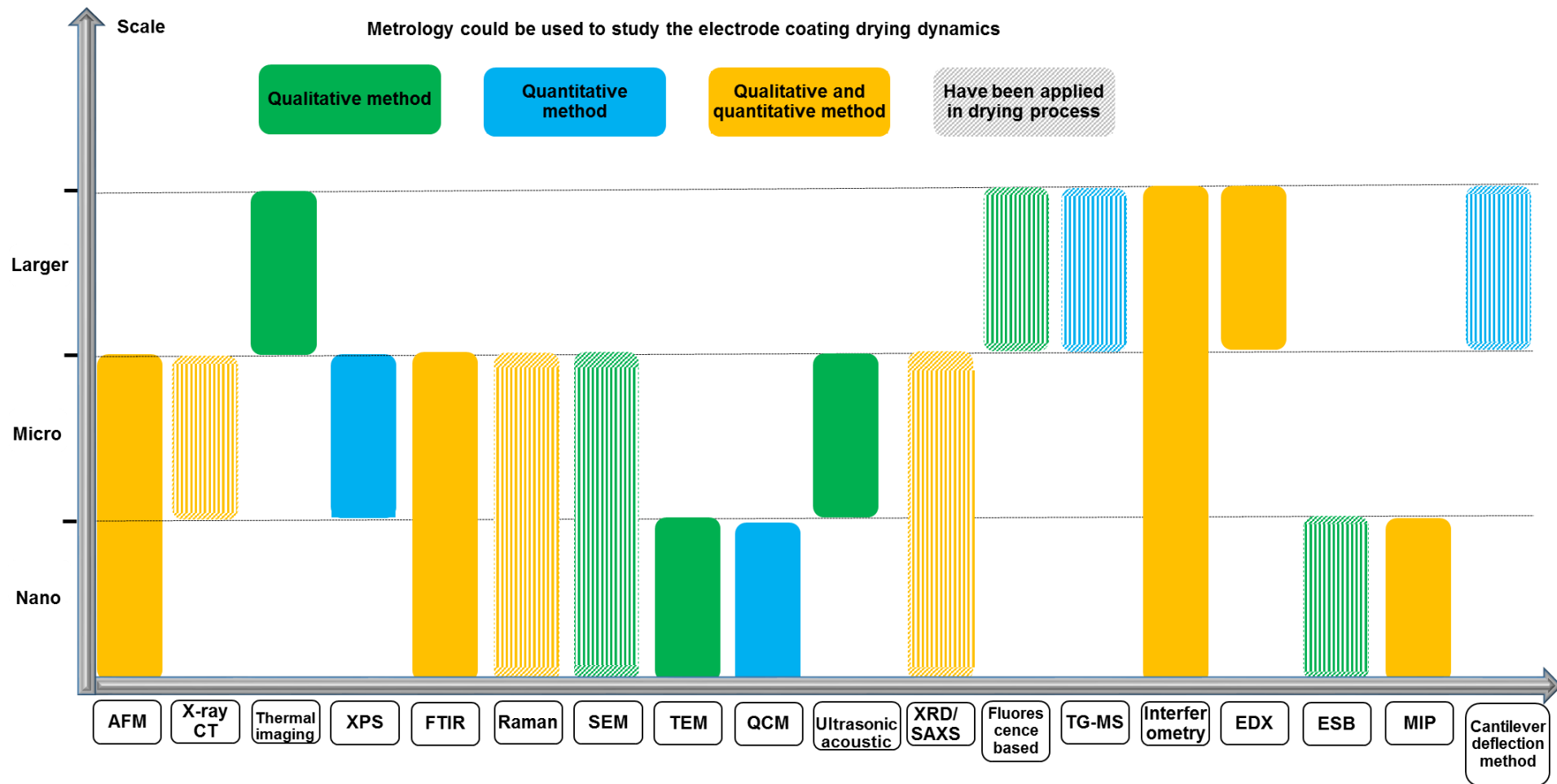
Figure 7 A summary of techniques have been used to study the electrode DP and the potential techniques that could be introduced to study the process.

Author contributions

D.J.L.B., E.K., Y.S.Z. conceived the idea. Y.S.Z., N.C., Z.Z. and K.L. conducted the literature review and wrote the manuscript. D.J.L.B., P.R.S., J.J.B., A.B., and G.R. discussed and revised the manuscript. E.K., D.J.L.B. and P.R.S. reviewed and edited the manuscript.

Declaration of interests

There are no conflicts to declare.

Acknowledgement

References:

[1]   GVR, *Grand View Research*, 2020.

[2]   H. Kim, J. Yoon, W.-S. Yoon, *ECS Meeting Abstracts* **2020**, 544.

[3]   E. Kendrick, in *Future Lithium-ion Batteries* **2019**, p. 262.

[4]   T. Danner, S. Hein, D. Westhoff, B. Prifling, V. Schmidt, A. Latz, *InterPore 2019* **2019**.

[5]   a) S. Nowak, M. Winter, *Journal of Analytical Atomic Spectrometry* **2017**, 32, 1833; b) P. Bieker, M. Winter, *Chemie in unserer Zeit* **2016**, 50, 172; c) L. Froboese, P. Titscher, B. Westphal, W. Haselrieder, A. Kwade, *Materials Characterization* **2017**, 133, 102; d) A. Kwade, W. Haselrieder, R. Leithoff, A. Modlinger, F. Dietrich, K. Droeder, *Nature Energy* **2018**, 3, 290; e) J. Vetter, P. Novák, M. R. Wagner, C. Veit, K.-C. Möller, J. Besenhard, M. Winter, M. Wohlfahrt-Mehrens, C. Vogler, A. Hammouche, *Journal of power sources* **2005**, 147, 269.

[6]   a) M. Xu, B. Reichman, X. Wang, *Energy* **2019**, 186, 115864; b) W. B. Hawley, J. Li, *Journal of Energy Storage* **2019**, 25, 100862.

[7]   a) M. Baunach, S. Jaiser, S. Schmelzle, H. Nirschl, P. Scharfer, W. Schabel, *Drying technology* **2016**, 34, 462; b) B. Westphal, H. Bockholt, T. Günther, W. Haselrieder, A.

Kwade, *ECS Transactions* **2015**, 64, 57; c) D. J. Harris, J. A. Lewis, *Langmuir* **2008**, 24, 3681.

[8]   S. Jaiser, M. Müller, M. Baunach, W. Bauer, P. Scharfer, W. Schabel, *Journal of Power Sources* **2016**, 318, 210.

[9]   D. L. Wood III, J. Li, C. Daniel, *Journal of Power Sources* **2015**, 275, 234.

[10]   C. Yuan, Y. Deng, T. Li, F. Yang, *CIRP Annals* **2017**, 66, 53.

[11]   D. L. Wood, J. D. Quass, J. Li, S. Ahmed, D. Ventola, C. Daniel, *Drying Technology* **2018**, 36, 234.

[12]   J. Li, Z. Du, R. E. Ruther, S. J. An, L. A. David, K. Hays, M. Wood, N. D. Phillip, Y. Sheng, C. Mao, *JOM* **2017**, 69, 1484.

[13]   a) R. Dominko, M. Gaberscek, J. Drofenik, M. Bele, S. Pejovnik, J. Jamnik, *Journal of Power Sources* **2003**, 119-121, 770; b) G.-W. Lee, J. H. Ryu, W. Han, K. H. Ahn, S. M. Oh, *Journal of Power Sources* **2010**, 195, 6049; c) H. Zheng, L. Zhang, G. Liu, X. Song, V. S. Battaglia, *Journal of Power Sources* **2012**, 217, 530; d) H. Bockholt, W. Haselrieder, A. Kwade, *ECS Transactions* **2013**, 50, 25; e) V. Wenzel, R. S. Moeller, H. Nirschl, *Energy Technology* **2014**, 2, 176; f) K. M. Kim, W. S. Jeon, I. J. Chung, S. H. Chang, *Journal of Power Sources* **1999**, 83, 108; g) H. Bockholt, W. Haselrieder, A. Kwade, *Powder Technology* **2016**, 297, 266; h) Z. Liu, V. Battaglia, P. P. Mukherjee, *Langmuir* **2014**, 30, 15102; i) A. Kraytsberg, Y. Ein-Eli, *Advanced Energy Materials* **2016**, 6, 1600655.

[14]   a) W. Haselrieder, S. Ivanov, H. Y. Tran, S. Theil, L. Froböse, B. Westphal, M. Wohlfahrt-Mehrens, A. Kwade, *Progress in Solid State Chemistry* **2014**, 42, 157; b) P. Tanguy, F. Thibault, C. Dubois, A. Ait-Kadi, *Chemical Engineering Research and Design* **1999**, 77, 318; c) N. Adachi, M. Hashiba, O. Sakurada, *Ceramics International* **2004**, 30, 1055; d) A. Kvasha, I. Urdampilleta, I. de Meatza, M. Bengoechea, J. A.

Blázquez, L. Yate, O. Miguel, H.-J. Grande, *Electrochimica Acta* **2016**, 215, 238; e) T. Chartrel, M. Ndour, V. Bonnet, S. Cavalaglio, L. Aymard, F. Dolhem, L. Monconduit, J.-P. Bonnet, *Materials Chemistry Frontiers* **2019**, 3, 881; f) C. Schilde, C. Mages-Sauter, A. Kwade, H. Schuchmann, *Powder technology* **2011**, 207, 353; g) C. Sauter, M. Emin, H. Schuchmann, S. Tavman, *Ultrasonics Sonochemistry* **2008**, 15, 517.

[15] a) M. Schmitt, M. Baunach, L. Wengeler, K. Peters, P. Junges, P. Scharfer, W. Schabel, *Chemical Engineering and Processing: Process Intensification* **2013**, 68, 32; b) M. Schmitt, P. Scharfer, W. Schabel, *Journal of Coatings Technology and Research* **2014**, 11, 57; c) X. Ding, J. Liu, T. A. L. Harris, *AIChE Journal* **2016**, 62, 2508; d) D. Mohanty, E. Hockaday, J. Li, D. K. Hensley, C. Daniel, D. L. Wood, *Journal of Power Sources* **2016**, 312, 70; e) D. Mohanty, J. Li, R. Born, L. C. Maxey, R. B. Dinwiddie, C. Daniel, I. I. I. D. L. Wood, *Analytical Methods* **2014**, 6, 674; f) A. Etiemble, N. Besnard, J. Adrien, P. Tran-Van, L. Gautier, B. Lestriez, E. Maire, *Journal of Power Sources* **2015**, 298, 285; g) R. Diehm, J. Kumberg, C. Dörrer, M. Müller, W. Bauer, P. Scharfer, W. Schabel, *Energy Technology* **2020**, 8, 1901251.

[16] a) C.-C. Li, Y.-W. Wang, *Journal of The Electrochemical Society* **2011**, 158, A1361; b) S. Lim, K. H. Ahn, M. Yamamura, *Langmuir* **2013**, 29, 8233; c) H. Hagiwara, W. J. Suszynski, L. F. Francis, *Journal of Coatings Technology and Research* **2014**, 11, 11; d) S. Jaiser, A. Friske, M. Baunach, P. Scharfer, W. Schabel, *Drying Technology* **2017**, 35, 1266; e) S. Jaiser, L. Funk, M. Baunach, P. Scharfer, W. Schabel, *Journal of Colloid and Interface Science* **2017**, 494, 22; f) S. Jaiser, J. Kumberg, J. Klaver, J. L. Urai, W. Schabel, J. Schmatz, P. Scharfer, *Journal of Power Sources* **2017**, 345, 97; g) M. Müller, L. Pfaffmann, S. Jaiser, M. Baunach, V. Trouillet, F. Scheiba, P. Scharfer, W. Schabel, W. Bauer, *Journal of Power Sources* **2017**, 340, 1; h) L. Pfaffmann, S. Jaiser, M. Müller, P. Scharfer, W. Schabel, W. Bauer, F. Scheiba, H. Ehrenberg, *Journal of Power Sources*

2017, 363, 460; i) N. Susarla, S. Ahmed, D. W. Dees, *Journal of Power Sources* **2018**, 378, 660.

[17]   a) Y. H. Chen, C. W. Wang, X. Zhang, A. M. Sastry, *Journal of Power Sources* **2010**, 195, 2851; b) W. Haselrieder, S. Ivanov, D. K. Christen, H. Bockholt, A. Kwade, *ECS Transactions* **2013**, 50, 59; c) I. V. Thorat, D. E. Stephenson, N. A. Zacharias, K. Zaghib, J. N. Harb, D. R. Wheeler, *Journal of Power Sources* **2009**, 188, 592; d) M. Ebner, D.-W. Chung, R. E. García, V. Wood, *Advanced Energy Materials* **2014**, 4, 1301278; e) D.-W. Chung, M. Ebner, D. R. Ely, V. Wood, R. Edwin García, *Modelling and Simulation in Materials Science and Engineering* **2013**, 21, 074009; f) T. Günther, D. Schreiner, A. Metkar, C. Meyer, A. Kwade, G. Reinhart, *Energy Technology* **2020**, 8, 1900026; g) D. Jeong, J. Lee, *Energy* **2014**, 75, 525; h) Y. Sheng, C. R. Fell, Y. K. Son, B. M. Metz, J. Jiang, B. C. Church, *Frontiers in Energy Research* **2014**, 2, 56; i) A. Schilling, J. Schmitt, F. Dietrich, K. Dröder, *Energy Technology* **2016**, 4, 1502; j) H. Bockholt, M. Indrikova, A. Netz, F. Golks, A. Kwade, *Journal of Power Sources* **2016**, 325, 140; k) H. Zheng, L. Tan, G. Liu, X. Song, V. S. Battaglia, *Journal of Power Sources* **2012**, 208, 52.

[18]   a) F. Huttner, W. Haselrieder, A. Kwade, *Energy Technology* **2020**, 8, 1900245; b) M. Stich, N. Pandey, A. Bund, *Journal of Power Sources* **2017**, 364, 84; c) K. Zaghib, M. Dontigny, P. Charest, J. Labrecque, A. Guerfi, M. Kopec, A. Mauger, F. Gendron, C. Julien, *Journal of Power Sources* **2008**, 185, 698; d) D. Aurbach, B. Markovsky, G. Salitra, E. Markevich, Y. Talyossef, M. Koltypin, L. Nazar, B. Ellis, D. Kovacheva, *Journal of Power Sources* **2007**, 165, 491; e) D. Aurbach, I. Weissman, A. Zaban, P. Dan, *Electrochimica acta* **1999**, 45, 1135; f) V. Saharan, J. Roberts, V. Manev, Y. H. Chia, G. MacLean, S. R. McMullen, *Journal of Power Sources* **2005**, 146, 809.

[19]   a) J. Kaiser, V. Wenzel, H. Nirschl, B. Bitsch, N. Willenbacher, M. Baunach, M. Schmitt, S. Jaiser, P. Scharfer, W. Schabel, *Chemie Ingenieur Technik* **2014**, 86, 695; b) T. Günther, N. Billot, J. Schuster, J. Schnell, F. B. Spingler, H. A. Gasteiger, presented at *Advanced Materials Research* **2016**.

[20]   Z. Liu, P. P. Mukherjee, *Journal of The Electrochemical Society* **2014**, 161, E3248.

[21]   B. G. Westphal, A. Kwade, *Journal of Energy Storage* **2018**, 18, 509.

[22]   a) M. Yoo, C. W. Frank, S. Mori, *Chemistry of materials* **2003**, 15, 850; b) M. Yoo, C. W. Frank, S. Mori, S. Yamaguchi, *Chemistry of Materials* **2004**, 16, 1945.

[23]   a) M. Stein, A. Mistry, P. P. Mukherjee, *Journal of The Electrochemical Society* **2017**, 164, A1616; b) E. S. Carreras, F. Chabert, D. Dunstan, G. Franks, *Journal of Colloid and Interface Science* **2007**, 313, 160; c) P. Xu, A. Mujumdar, B. Yu, *Drying Technology* **2009**, 27, 636.

[24]   F. Font, B. Protas, G. Richardson, J. M. Foster, *Journal of Power Sources* **2018**, 393, 177.

[25]   H. Luo, C. M. Cardinal, L. Scriven, L. F. Francis, *Langmuir* **2008**, 24, 5552.

[26]   J. Kumberg, M. Müller, R. Diehm, S. Spiegel, C. Wachsmann, W. Bauer, P. Scharfer, W. Schabel, *Energy Technology* **2019**, 7, 1900722.

[27]   Y. Garsany, I. L. Singer, K. E. Swider-Lyons, *Journal of Electroanalytical Chemistry* **2011**, 662, 396.

[28]   Y. Garsany, O. A. Baturina, K. E. Swider-Lyons, S. S. Kocha, *Analytical Chemistry* **2010**, 82, 6321.

[29]   a) D. S. Jung, T. H. Hwang, S. B. Park, J. W. Choi, *Nano letters* **2013**, 13, 2092; b) H. Wu, J. Tu, Y. Yuan, Y. Li, X. Zhao, G. Cao, *Materials Science and Engineering: B* **2005**, 119, 75; c) J. H. Kim, Y. S. Jang, B. K. Park, Y. C. Kang, *International Journal of Electrochemical Science* **2013**, 8, 1067; d) G. Zhou, D.-W. Wang, X. Shan, N. Li, F.

Li, H.-M. Cheng, *Journal of Materials Chemistry* **2012**, 22, 11252; e) X. Du, Z. Jiang, X. Meng, Z. Wang, H. Yu, M. Li, T. Tang, *The Journal of Physical Chemistry C* **2008**, 112, 6638; f) A. Gharsallaoui, G. Roudaut, O. Chambin, A. Voilley, R. Saurel, *Food Research International* **2007**, 40, 1107; g) F. Iskandar, A. B. D. Nandiyanto, K. M. Yun, C. J. Hogan Jr., K. Okuyama, P. Biswas, *Advanced Materials.* **2007**, 19, 1408; h) G. D. Park, J. H. Kim, Y. J. Choi, Y. C. Kang, *Electrochimica Acta* **2015**, 173, 581.

[30]   D. Hawelka, J. Stollenwerk, N. Pirch, L. Büsing, K. Wissenbach, *Physics Procedia* **2011**, 12, 490.

[31]   B. Barnett, J. Rempel, C. McCoy, S. Dalton-Castor, S. Sriramulu, *DOE Annual Merit Review* **2011**.

[32]   F. Scheepers, A. Stähler, M. Stähler, M. Carmo, W. Lehnert, D. Stolten, *Journal of Coatings Technology and Research* **2019**, 16, 1213.

[33]   A. Gören, D. Cíntora-Juárez, P. Martins, S. Ferdov, M. M. Silva, J. L. Tirado, C. M. Costa, S. Lanceros-Méndez, *Energy Technology* **2016**, 4, 573.

[34]   M.-H. Tsai, J.-L. Hong, *Electrochimica Acta* **2020**, 359, 136967.

[35]   J. Li, Y. Lu, T. Yang, D. Ge, D. L. Wood, Z. Li, *iScience* **2020**, 23, 101081.

[36]   a) J.-H. Lee, S. Lee, U. Paik, Y.-M. Choi, *Journal of Power Sources* **2005**, 147, 249; b) W. Porcher, B. Lestriez, S. Jouanneau, D. Guyomard, *Journal of the Electrochemical Society.* **2009**, 156, A133; c) J.-H. Lee, J.-S. Kim, Y. C. Kim, D. S. Zang, U. Paik, *Ultramicroscopy* **2008**, 108, 1256; d) C.-C. Li, J.-T. Lee, C.-Y. Lo, M.-S. Wu, *Electrochemical and Solid-State Letters* **2005**, 8, A509; e) J.-H. Lee, U. Paik, V. A. Hackley, Y.-M. Choi, *Journal of Power Sources* **2006**, 161, 612; f) C.-C. Li, J.-T. Lee, X.-W. Peng, *Journal of the Electrochemical Society* **2006**, 153, A809; g) J. Li, B. L. Armstrong, J. Kiggans, C. Daniel, D. L. Wood III, *Langmuir* **2012**, 28, 3783; h) J. Li, B. L. Armstrong, C. Daniel, J. Kiggans, D. L. Wood III, *Journal of Colloid and*

Interface Science **2013**, 405, 118; i) W. Porcher, B. Lestriez, S. Jouanneau, D. Guyomard, *Journal of Power Sources* **2010**, 195, 2835; j) S. Lim, S. Kim, K. H. Ahn, S. J. Lee, *Journal of Power Sources* **2015**, 299, 221; k) C.-C. Li, X.-W. Peng, J.-T. Lee, F.-M. Wang, *Journal of the Electrochemical Society* **2010**, 157, A517.

[37] J. Li, Z. Du, R. E. Ruther, S. J. An, L. A. David, K. Hays, M. Wood, N. D. Phillip, Y. Sheng, C. Mao, S. Kalnaus, C. Daniel, D. L. Wood, *JOM* **2017**, 69, 1484.

[38] a) M. Zackrisson, L. Avellán, J. Orlenius, *Journal of Cleaner Production* **2010**, 18, 1519; b) J.-H. Lee, U. Paik, V. A. Hackley, Y.-M. Choi, *Journal of The Electrochemical Society* **2005**, 152, A1763.

[39] S. Tsantilis, S. E. Pratsinis, *Langmuir* **2004**, 20, 5933.

[40] a) J. Li, C. Daniel, D. Wood, *Journal of Power Sources* **2011**, 196, 2452; b) Z. Du, K. Rollag, J. Li, S. J. An, M. Wood, Y. Sheng, P. Mukherjee, C. Daniel, D. Wood Iii, *Journal of Power Sources* **2017**, 354, 200.

[41] a) I. Doberdò, N. Löffler, N. Laszczynski, D. Cericola, N. Penazzi, S. Bodoardo, G.-T. Kim, S. Passerini, *Journal of power sources* **2014**, 248, 1000; b) M. Kuenzel, D. Bresser, T. Diemant, D. V. Carvalho, G. T. Kim, R. J. Behm, S. Passerini, *ChemSusChem* **2018**, 11, 562.

[42] B. C. Church, D. T. Kaminski, J. Jiang, *Journal of Materials Science* **2014**, 49, 3234.

[43] C. Wang, H. Wu, Z. Chen, M. T. McDowell, Y. Cui, Z. Bao, *Nature Chemistry* **2013**, 5, 1042.

[44] D. Liu, Y. Zhao, R. Tan, L.-L. Tian, Y. Liu, H. Chen, F. Pan, *Nano Energy* **2017**, 36, 206.

[45] T. Danner, M. Singh, S. Hein, J. Kaiser, H. Hahn, A. Latz, *Journal of Power Sources* **2016**, 334, 191.

[46]   H. Zheng, R. Yang, G. Liu, X. Song, V. S. Battaglia, *The Journal of Physical Chemistry C* **2012**, 116, 4875.

[47]   M. M. Forouzan, C.-W. Chao, D. Bustamante, B. A. Mazzeo, D. R. Wheeler, *Journal of Power Sources* **2016**, 312, 172.

[48]   M. Westermeier, G. Reinhart, T. Zeilinger, presented at 2013 3rd International Electric Drives Production Conference (EDPC) **2013**.

[49]   J. Schnell, C. Nentwich, F. Endres, A. Kollenda, F. Distel, T. Knoche, G. Reinhart, *Journal of Power Sources* **2019**, 413, 360.

[50]   A. Turetskyy, S. Thiede, M. Thomitzek, N. von Drachenfels, T. Pape, C. Herrmann, *Energy Technology* **2020**, 8, 1900136.

[51]   R. P. Cunha, T. Lombardo, E. N. Primo, A. A. Franco, *Batteries & Supercaps* **2020**.

[52]   a) Y.-H. Zang, J. Du, Y. Du, Z. Wu, S. Cheng, Y. Liu, *Langmuir* **2010**, 26, 18331; b) A. K. Atmuri, S. R. Bhatia, A. F. Routh, *Langmuir* **2012**, 28, 2652.

[53]   A. Kumar1, R. P. , a. Y. C. Sharma3, *International Journal of Environmental Research and Development* **2014**, 4, 203.

[54]   A. M. Tripathi, W.-N. Su, B. J. Hwang, *Chemical Society Reviews* **2018**, 47, 736.

[55]   X. Lu, A. Bertei, D. P. Finegan, C. Tan, S. R. Daemi, J. S. Weaving, K. B. O'Regan, T. M. Heenan, G. Hinds, E. Kendrick, *Nature Communications* **2020**, 11, 1.

[56]   a) K.-i. Morigaki, *Journal of power sources* **2002**, 104, 13; b) R. Vidu, P. Stroeve, *Industrial & Engineering Chemistry Research* **2004**, 43, 3314; c) B. Fleutot, H. Martinez, B. Pecquenard, J.-B. Ledeuil, A. Levasseur, D. Gonbeau, *Journal of Power Sources* **2008**, 180, 836; d) Z. Zhang, K. Smith, R. Jervis, P. R. Shearing, T. S. Miller, D. J. L. Brett, *ACS Applied Materials & Interfaces* **2020**, 12, 35132.

[57]   a) M. Krieg, G. Fläschner, D. Alsteens, B. M. Gaub, W. H. Roos, G. J. Wuite, H. E. Gaub, C. Gerber, Y. F. Dufrêne, D. J. Müller, *Nature Reviews Physics* **2019**, 1, 41; b)

K. Xu, W. Sun, Y. Shao, F. Wei, X. Zhang, W. Wang, P. Li, *Nanotechnology Reviews* **2018**, 7, 605; c) H. Shin, J. Park, S. Han, A. M. Sastry, W. Lu, *Journal of Power Sources* **2015**, 277, 169.

[58]   P. J. Whiteside, J. A. Chininis, H. K. Hunt, *Coatings* **2016**, 6, 35.

[59]   X. Chen, J. Lai, Y. Shen, Q. Chen, L. Chen, *Advanced Materials.* **2018**, 30, 1802490.

[60]   S. Lim, S. Kim, K. H. Ahn, S. J. Lee, *Industrial & Engineering Chemistry Research* **2015**, 54, 6146.

[61]   a) S. Kim, J. H. Sung, K. Hur, K. H. Ahn, S. J. Lee, *J. Colloid Interface Sci.* **2010**, 344, 308; b) S. Kim, J. Sung, K. Ahn, S. Lee, *Langmuir* **2009**, 25, 6155.

[62]   a) G. Bohn, J. Taub, A. Linke, S. Bayer, D. Oeser, A. Ziegler, P. Ettl, A. Ackva, presented at IOP Conference Series: Earth and Environmental Science **2019**; b) A. Yoneyama, *Hyomen To Shinku (Online)* **2019**, 62, 92; c) D. Takamatsu, A. Yoneyama, Y. Asari, T. Hirano, *Journal of the American Chemical Society* **2018**, 140, 1608.

[63]   a) F. Bahiraei, M. Ghalkhani, A. Fartaj, G.-A. Nazri, *Applied Thermal Engineering* **2017**, 125, 904; b) S. Goutam, J.-M. Timmermans, N. Omar, P. V. d. Bossche, J. Van Mierlo, *Energies* **2015**, 8, 8175; c) K. Murashko, J. Pyrhönen, L. Laurila, *IEEE Transactions on Energy Conversion* **2013**, 28, 335; d) S. Kosch, A. Rheinfeld, S. V. Erhard, A. Jossen, *Journal of Power Sources* **2017**, 342, 666; e) D. P. Finegan, M. Scheel, J. B. Robinson, B. Tjaden, I. Hunt, T. J. Mason, J. Millichamp, M. Di Michiel, G. J. Offer, G. Hinds, *Nature Communications* **2015**, 6, 6924; f) J. B. Robinson, J. A. Darr, D. S. Eastwood, G. Hinds, P. D. Lee, P. R. Shearing, O. O. Taiwo, D. J. Brett, *Journal of Power Sources* **2014**, 252, 51; g) J. B. Robinson, E. Engebretsen, D. P. Finegan, J. Darr, G. Hinds, P. R. Shearing, D. J. Brett, *ECS Electrochemistry Letters* **2015**, 4, A106.

[64] a) K.-P. Möllmann, M. Vollmer, *European Journal of Physics* **2007**, 28, S37; b) L. H. J. Raijmakers, D. L. Danilov, R. A. Eichel, P. H. L. Notten, *Applied Energy* **2019**, 240, 918.

[65] M. Vollmer, K.-P. Möllmann, *Infrared thermal imaging: Fundamentals, Research and Applications*, John Wiley & Sons, **2017**.

[66] S. Panchal, I. Dincer, M. Agelin-Chaab, R. Fraser, M. Fowler, *Applied Energy* **2016**, 180, 504.

[67] a) D. Cumming, R. Elder, *Journal of Power Sources* **2015**, 280, 387; b) M. B. Pomfret, D. A. Steinhurst, D. A. Kidwell, J. C. Owrutsky, *Journal of Power Sources* **2010**, 195, 257.

[68] a) T. Narita, C. Beauvais, P. Hébraud, F. Lequeux, *The European Physical Journal E* **2004**, 14, 287; b) P. Zakharov, F. Scheffold, *Soft Materials* **2010**, 8, 102; c) L. Xu, S. Davies, A. B. Schofield, D. A. Weitz, *Physical Review Letters* **2008**, 101, 094502; d) E. R. Dufresne, E. I. Corwin, N. Greenblatt, J. Ashmore, D. Wang, A. D. Dinsmore, J. Cheng, X. Xie, J. W. Hutchinson, D. A. Weitz, *Physical Review Letters* **2003**, 91, 224501; e) M. Bellour, A. Knaebel, J. Harden, F. Lequeux, J.-P. Munch, *Physical Review E* **2003**, 67, 031405; f) J. Harden, V. Viasnoff, *Current opinion in colloid & interface science* **2001**, 6, 438; g) V. Viasnoff, F. Lequeux, D. Pine, *Review of Scientific Instruments* **2002**, 73, 2336; h) P. Zakharov, F. Cardinaux, F. Scheffold, *Physical Review E* **2006**, 73, 011413; i) L. Brunel, A. Brun, P. Snabre, L. Cipelletti, *Optics Express* **2007**, 15, 15250; j) G. Maret, P. Wolf, *Zeitschrift für Physik B Condensed Matter* **1987**, 65, 409; k) S. E. Skipetrov, J. Peuser, R. Cerbino, P. Zakharov, B. Weber, F. Scheffold, *Optics Express* **2010**, 18, 14519.

[69] J. Y. Lee, J. W. Hwang, H. W. Jung, S. H. Kim, S. J. Lee, K. Yoon, D. A. Weitz, *Langmuir* **2013**, 29, 861.

[70]   a) Y. Reynier, R. Yazami, B. Fultz, *Journal of Power Sources* **2007**, 165, 616; b) J. Światowska, V. Lair, C. Pereira-Nabais, G. Cote, P. Marcus, A. Chagnes, *Applied Surface Science* **2011**, 257, 9110; c) W.-w. Liu, X.-b. Yan, J.-w. Lang, C. Peng, Q.-j. Xue, *Journal of Materials Chemistry* **2012**, 22, 17245.

[71]   M. D. Levi, E. A. Levi, D. Aurbach, *Journal of Electroanalytical Chemistry* **1997**, 421, 89.

[72]   J. Dahn, R. Fong, M. Spoon, *Physical Review B* **1990**, 42, 6424.

[73]   T. Zemb, P. Lindner, *Neutrons, X-rays and light: scattering methods applied to soft condensed matter*, North-Holland, **2002**.

[74]   D. Sen, O. Spalla, O. Taché, P. Haltebourg, A. Thill, *Langmuir* **2007**, 23, 4296.

[75]   J. Li, B. Cabane, M. Sztucki, J. Gummel, L. Goehring, *Langmuir* **2012**, 28, 200.

[76]   B. Struth, K. Hyun, E. Kats, T. Meins, M. Walther, M. Wilhelm, G. Grübel, *Langmuir* **2011**, 27, 2880.

[77]   S. Kim, K. Hyun, Y. S. Kim, B. Struth, C. Clasen, K. H. Ahn, *Langmuir* **2013**, 29, 10059.

[78]   T. Kusano, T. Hiroi, K. Amemiya, M. Ando, T. Takahashi, M. Shibayama, *Polymer Journal* **2015**, 47, 546.

[79]   a) R. Baddour-Hadjean, J.-P. Pereira-Ramos, *Chemical reviews* **2010**, 110, 1278; b) M. Delhaye, P. Dhamelincourt, *Journal of Raman Spectroscopy* **1975**, 3, 33; c) M. Delhaye, M. Bridoux, F. Wallart, *Journal of Molecular Structure* **1982**, 79, 51.

[80]   a) S.-W. Hwang, S.-H. Hyun, *Journal of Power Sources* **2007**, 172, 451; b) H. Luo, C. M. Cardinal, L. E. Scriven, L. F. Francis, *Langmuir* **2008**, 24, 5552; c) Y. Ma, H. T. Davis, L. E. Scriven, *Prog. Org. Coat.* **2005**, 52, 46; d) F. Buss, C. C. Roberts, K. S. Crawford, K. Peters, L. F. Francis, *Journal of Colloid and Interface Science* **2011**, 359, 112.

[81]   F. M. Ross, *Science* **2015**, 350.

[82]   H. Jaksch, *EMAS conference* **2011**.

[83]   J. Millichamp, T. J. Mason, N. P. Brandon, R. J. Brown, R. C. Maher, G. Manos, T. P. Neville, D. J. Brett, *J. Power Sources* **2013**, 235, 14.

[84]   Y. S. Zhang, *ACS Applied Materials & Interfaces* **2021**, 13, 36605.

[85]   K. Higa, H. Zhao, D. Y. Parkinson, H. Barnard, M. Ling, G. Liu, V. Srinivasan, *Journal of The Electrochemical Society* **2017**, 164, A380.

[86]   a) D. Westhoff, I. Manke, V. Schmidt, *Computational Materials Science* **2018**, 151, 53; b) D. Zhang, A. Forner-Cuenca, O. O. Taiwo, V. Yufit, F. R. Brushett, N. P. Brandon, S. Gu, Q. Cai, *Journal of Power Sources* **2020**, 447, 227249; c) C. Rahe, S. T. Kelly, M. N. Rad, D. U. Sauer, J. Mayer, E. Figgemeier, *Journal of Power Sources* **2019**, 433, 126631.

[87]   R. F. Ziesche, T. Arlt, D. P. Finegan, T. M. Heenan, A. Tengattini, D. Baum, N. Kardjilov, H. Markötter, I. Manke, W. Kockelmann, *Nature Communications* **2020**, 11, 1.

[88]   M. Ebner, F. Geldmacher, F. Marone, M. Stampanoni, V. Wood, *Advanced Energy Materials* **2013**, 3, 845.

[89]   O. O. Taiwo, D. P. Finegan, D. S. Eastwood, J. L. Fife, L. D. Brown, J. A. Darr, P. D. Lee, D. J. Brett, P. R. Shearing, *Journal of Microscopy* **2016**, 263, 280.

[90]   a) S. Müller, J. Eller, M. Ebner, C. Burns, J. Dahn, V. Wood, *Journal of The Electrochemical Society* **2018**, 165, A339; b) R. E. García, Y.-M. Chiang, W. C. Carter, P. Limthongkul, C. M. Bishop, *Journal of The Electrochemical Society* **2005**, 152, A255.

[91]   B. Song, I. Dhiman, J. C. Carothers, G. M. Veith, J. Liu, H. Z. Bilheux, A. Huq, *ACS Energy Letters* **2019**, 4, 2402.

[92]   F. C. Krebs, *Solar Energy Materials and Solar Cells* **2009**, 93, 465.

[93]   E. Peled, *Journal of The Electrochemical Society* **1979**, 126, 2047.

[94]   a) M. Inaba, H. Yoshida, Z. Ogumi, T. Abe, Y. Mizutani, M. Asano, *Journal of The Electrochemical Society* **1995**, 142, 20; b) C. Sole, N. E. Drewett, L. J. Hardwick, *Faraday discussions* **2014**, 172, 223; c) W. Tang, B.-M. Goh, M. Y. Hu, C. Wan, B. Tian, X. Deng, C. Peng, M. Lin, J. Z. Hu, K. P. Loh, *The Journal of Physical Chemistry C* **2016**, 120, 2600.

[95]   K. Ni, X. Wang, Z. Tao, J. Yang, N. Shu, J. Ye, F. Pan, J. Xie, Z. Tan, X. Sun, *Advanced Materials.* **2019**, 31, 1808091.

[96]   Y. Han, Y. Jie, F. Huang, Y. Chen, Z. Lei, G. Zhang, X. Ren, L. Qin, R. Cao, S. Jiao, *Advanced Functional Materials* **2019**, 29, 1904629.

[97]   a) S. Chattopadhyay, A. L. Lipson, H. J. Karmel, J. D. Emery, T. T. Fister, P. A. Fenter, M. C. Hersam, M. J. Bedzyk, *Chemistry of Materials* **2012**, 24, 3038; b) J. Gao, M. Yoshio, L. Qi, H. Wang, *Journal of Power Sources* **2015**, 278, 452.

[98]   K. Qian, R. E. Winans, T. Li, *Advanced Energy Materials* **2021**, 11, 2002821.

[99]   a) P. G. Kitz, P. Novák, E. J. Berg, *ACS Applied Materials & Interfaces* **2020**, 12, 15934; b) V. Dargel, N. Shpigel, S. Sigalov, P. Nayak, M. D. Levi, L. Daikhin, D. Aurbach, *Nature Communications* **2017**, 8, 1; c) P. G. Kitz, M. J. Lacey, P. Novák, E. J. Berg, *Analytical Chemistry* **2018**, 91, 2296; d) Z. Yang, M. C. Dixon, R. A. Erck, L. Trahey, *ACS Applied Materials & Interfaces* **2015**, 7, 26585.

[100]   a) S. Pérez-Villar, P. Lanz, H. Schneider, P. Novák, *Electrochimica Acta* **2013**, 106, 506; b) A. Viinikanoja, J. Kauppila, P. Damlin, M. Suominen, C. Kvarnström, *Physical Chemistry Chemical Physics* **2015**, 17, 12115.

[101]   a) A. Hsieh, S. Bhadra, B. Hertzberg, P. Gjeltema, A. Goy, J. W. Fleischer, D. A. Steingart, *Energy & Environmental Science* **2015**, 8, 1569; b) G. Davies, K. W. Knehr,

B. Van Tassell, T. Hodson, S. Biswas, A. G. Hsieh, D. A. Steingart, *Journal of The Electrochemical Society* **2017**, 164, A2746.

[102] C. Bommier, W. Chang, Y. Lu, J. Yeung, G. Davies, R. Mohr, M. Williams, D. Steingart, *Cell Reports Physical Science* **2020**, 1, 100035.

[103] J. B. Robinson, M. Maier, G. Alster, T. Compton, D. J. Brett, P. R. Shearing, *Physical Chemistry Chemical Physics* **2019**, 21, 6354.

[104] C. M. Cardinal, Y. D. Jung, K. H. Ahn, L. Francis, *AIChE journal* **2010**, 56, 2769.

[105] A. F. Routh, W. B. Zimmerman, *Chemical Engineering Science* **2004**, 59, 2961.

[106] S. Whitaker, in *Advances in heat transfer*, Vol. 13, Elsevier **1977**, p. 119.

[107] E. Tsotsas, A. S. Mujumdar, *Modern Drying Technology*, Wiley Online Library, **2007**.

[108] T. Metzger, *Drying Technology* **2019**, 37, 497.

[109] T. Defraeye, *Applied Energy* **2014**, 131, 323.

Dr. Yeshui Zhang is a Faraday Institution Research Fellow at University College London, UK since January 2018 and has been appointed as a Lecturer in Chemical Engineering at University of Aberdeen, UK in Dec 2021. She has completed her BSc. from University of Birmingham in 2012 and MSc. (Engineering) from The University of Sheffield in 2013. She finished her PhD in September 2017 at University of Leeds. Her research interests cover broad area of chemical engineering, including energy storage materials, lithium-ion battery manufacturing, pyrolysis-catalysis of waste, high temperature quartz crystal microbalance, carbon nanotubes synthesis and circular economy of plastics.

Dan Brett is a Professor of Electrochemical Engineering at University College London. Hs research is in the area if electrochemical engineering and technology. This includes electrochemical energy conversion and storage (fuel cells, batteries, supercapacitors, electrolysers), electrochemical sensors, electroanalysis, hybrid vehicles and micro-generation technologies. He specialises in developing novel diagnostic techniques for the study of high and low temperature fuel cells and their materials.

Emma Kendrick is Professor of Energy Materials. Professor Kendrick has worked in industry and academic extensively on energy materials and devices; batteries and fuel cells, and has 70 papers and 21 patent family applications in this field. Her recent book chapter on Advanced Battery manufacturing is being published by the RSC. Her research over the last 20 years has focused on translation of novel functional materials to industry relevant device demonstrators, new battery materials and chemistries to cell demonstrators. Her enthusiasm for new technology development, mainly batteries, extends to the industrial and academic fields.

Table of content
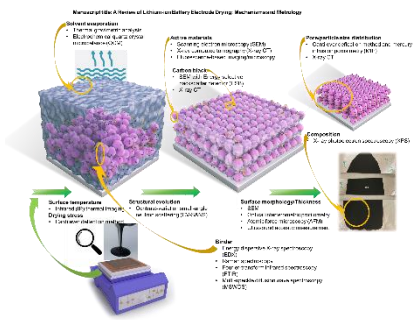
Reviewed metrology for characterizing the various properties of lithium-ion battery electrode at different stage of drying process.